MSEL

Materials Science and Engineering Laboratory

MATERIALS RELIABILITY

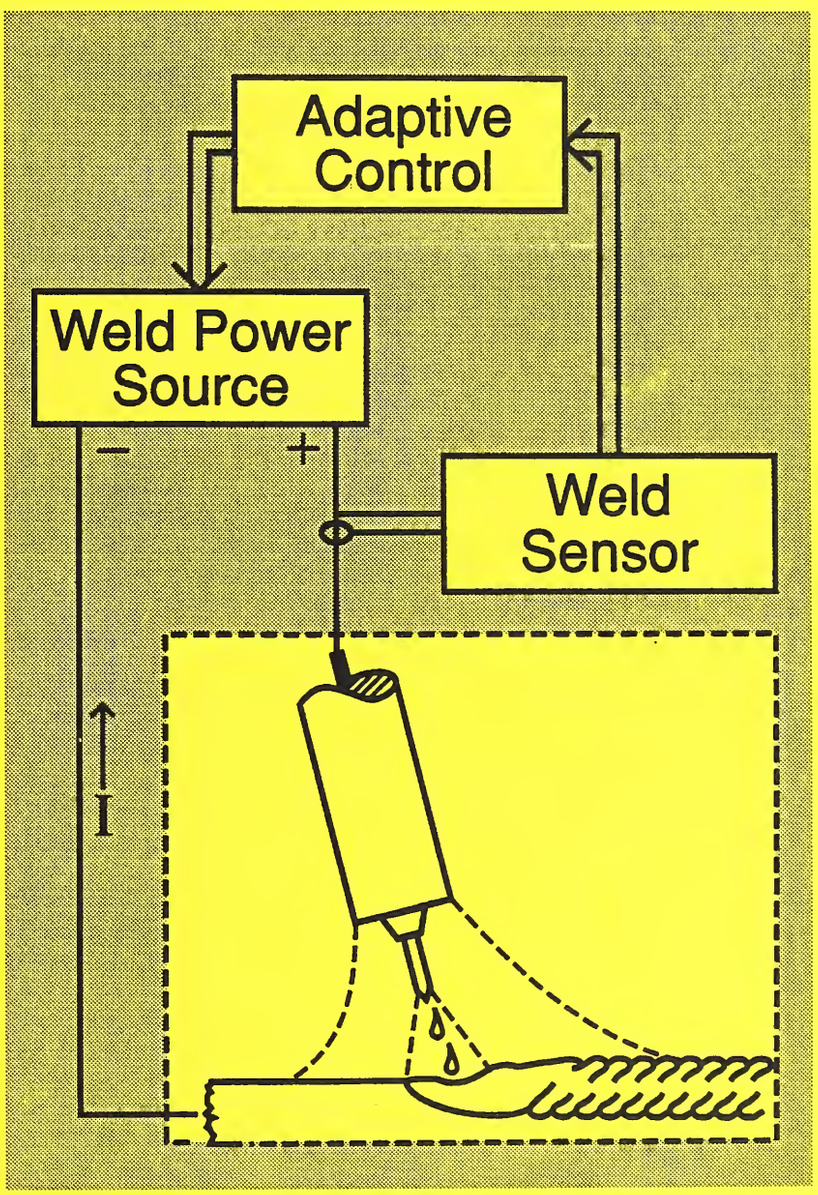

NAS-NRC
Assessment Panel
February 13-14, 1992

NISTIR 4695
U.S. Department of Commerce
National Institute of Standards
and Technology

Technical Activities 1991

Arc sensors and a process model are being developed for adaptive control of the gas metal arc welding process.

Materials Science and Engineering Laboratory

MATERIALS RELIABILITY

H.I. McHenry, Chief
C.M. Fortunko, Deputy

NAS-NRC
Assessment Panel
February 13-14, 1992

NISTIR 4695
U.S. Department of Commerce
National Institute of Standards
and Technology

Technical Activities 1991

U.S. DEPARTMENT OF COMMERCE, Robert A. Mosbacher,Secretary
National Institute of Standards and Technology, John W. Lyons, Director

CONTENTS

DIVISION ORGANIZATION

Harry I. McHenry, Chief
(303) 497-3268

Christopher M. Fortunko
Deputy Division Chief
(303) 497-3062

PERFORMANCE	
Fracture	David T. Read (303) 497-3853
Nondestructive Evaluation	Alfred V. Clark, Jr. (303) 497-3159
Composites	Christopher M. Fortunko (303) 497-3062
PROPERTIES	
Cryogenic Materials	Harry I. McHenry (Acting) (303) 497-3268
Physical Properties	Hassel M. Ledbetter (303) 497-3443
PROCESSING	
Welding	Thomas A. Siewert (303) 497-3523
Thermomechanical Processing	Yi-Wen Cheng (303) 497-5545
ADMINISTRATIVE SUPPORT	
Administrative Officer	Kathy S. Sherlock (303) 497-3288
Division Secretary	Heidi M. Quartemont (303) 497-3251
Group Secretaries	Vonna E. Ciaranello (303) 497-5338 Dawn T. Lewis (303) 497-3290

INTRODUCTION

MATERIALS RELIABILITY DIVISION

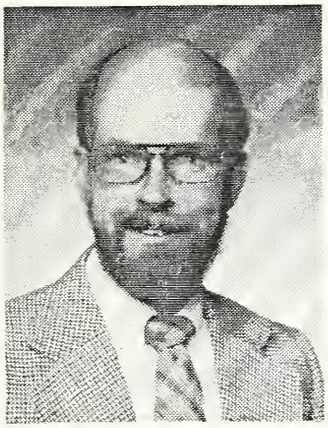

Harry I. McHenry
Chief

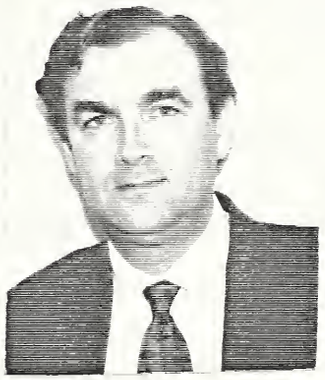

Christopher M. Fortunko
Deputy Chief

The Materials Reliability Division conducts materials research to improve the quality, reliability, and safety of industrial products and the nation's infrastructure. Our research fosters the use of advanced materials in commercial products by improving confidence in their service performance. We do this by developing measurement technology for:

1. process control which improves the quality, consistency and producibility of materials,

2. nondestructive evaluation (NDE) which assures the quality of finished materials and products,

3. fitness-for-purpose standards which relate material quality to reliability and safety, and

4. materials evaluation for severe applications, particularly for service at cryogenic temperatures.

Our interdisciplinary staff is organized into specific research groups in the general areas of materials performance, properties, and processing. Each group is headed by a recognized expert in that technology providing a focal point for industrial cooperations, scientific interactions, and technology transfer.

In support of the long-range plan of the Materials Science and Engineering Laboratory, our new programs focus on advanced materials with high commercial potential and on automated processing, which is the key to improved productivity in the materials industry. We also conduct materials research for other government agencies and provide technical services to industries, universities, and other scientific laboratories.

SELECTED HIGHLIGHTS
MATERIALS RELIABILITY DIVISION

Acoustic Microscopy: A high-pressure, gas-coupled acoustic microscope was designed, built, and demonstrated. Proof-of-concept experiments on silicon wafers showed excellent signal-to-noise and resolution potential below 10 μm.

NDE Instruments: A prototype residual stress measurement system for railroad wheels was developed, evaluated, and delivered to the American Association of Railroads for further evaluation in their Transportation Test Center.

Micrometer-Scale Testing: A micromechanical test apparatus was assembled and used for in-situ measurements of the strength and ductility of aluminum thin films deposited on a silicon substrate.

Thermomechanical Processing: A physical model to mathematically describe the flow behavior of microalloyed steels at high temperatures and high strain rates has been developed.

Intelligent Welding: An arc sensor module with algorithms for detecting various causes of weld defects has been developed for delivering to Babcock and Wilcox for integration into a programmable arc welding system.

Reference Radiographs: A series of reference radiographs on aluminum welds with controlled defect levels has been prepared and submitted to ASTM for standardization.

Materials Testing Standard: A standard method developed by NIST for conducting tension tests in liquid helium has been formally approved by ASTM.

Process Modelling: A heat transfer model of electrode melting in gas metal arc welding (GMAW) was developed for use in adaptive control of the metal deposition process.

Metal-Matrix Composites: The complete elastic constants for seven Al_2O_3/Al spherical-particle-reinforced composites were determined. Measurements and model agree quite well.

Moving Sheet Facility: A test bed to demonstrate the feasibility of on-line measurements of sheet steel formability using the NIST ultrasonic sensor system was developed in collaboration with Ford Motor Company.

Acoustic Arrays: An acoustic array consisting of a high-power, broad bandwidth point source and a linear array of high sensitivity point receivers has been designed and built. The initial experiments demonstrated excellent signal-to-noise ratio in thick glass/epoxy composites.

RESEARCH STAFF

Austin, Mark W.
- Radioscopy
- Elastic properties
- X-ray diffraction

Cheng, Yi-Wen
- Fatigue of metals
- Thermomechanical processing of steels
- Ferrous metallurgy

Clark, Alfred V., Jr.
- Ultrasonic NDE
- Engineering mechanics
- Nondestructive evaluation

Drexler, Elizabeth S.
- Materials properties at low temperatures
- Database management
- Composite materials testing

Fitting, Dale W.
- Sensor arrays for NDE
- Ultrasonic and radiographic NDE
- NDE of composites

Fortunko, Christopher M.
- Ultrasonic transducers and instrumentation
- Nondestructive evaluation
- Analog measurements

Kim, Sudook
- Elastic properties
- Low-temperature physical properties
- Ultrasonics

Ledbetter, Hassel M.
- Physical properties of solids
- Theory and measurement of elastic constants
- Martensite-transformation theory

Lin, Ing-Hour
- Electronic materials
- Physics of fracture
- Dislocation theory

Madigan, R. Bruce
- Welding engineering
- Welding process sensors
- Process control

McColskey, J. David
- Cryogenic materials
- Composite materials
- Mechanical testing

McCowan, Chris N.
- Welding metallurgy
- Mechanical properties at low temperatures
- Metallography and fractography

McHenry, Harry I.
- Fracture mechanics
- Low-temperature materials
- Fracture control

Purtscher, Patrick T.
- Fracture properties of metals
- Metallography and fractography
- Mechanical properties at low temperatures

Quinn, Timothy P.
- Control theory
- Welding automation
- Mechanical design

Read, David T.
- Electronic packaging
- Elastic–plastic fracture mechanics
- Mechanical properties of metals

Schaps, Stephen R.
- Electrical design
- Nondestructive evaluation
- Capacitance sensors

Schramm, Raymond E.
- Ultrasonic NDE of welds
- Ultrasonic measurement of residual stress
- Electromagnetic acoustic transducers

Shepherd, Dominique A.
- Charpy impact testing
- Metallography and fractography
- Thermomechanical processing

Siewert, Thomas A.
- Welding metallurgy of steel
- Gas–metal interactions during welding
- Welding database management

Simon, Nancy J.
- Material properties at low temperatures
- Database management of material properties
- Handbook of material properties

Tobler, Ralph L.
- Fracture mechanics
- Material properties at low temperatures
- Low-temperature test standards

Walsh, Robert P.
- Mechanical properties at low temperatures
- Mechanical test equipment
- Large scale testing

Yukawa, Sumio
- Fracture mechanics
- Codes and standards
- Structural safety

TECHNICAL ACTIVITIES

PERFORMANCE

The Nondestructive Evaluation, Composite Materials, and Fracture Groups work together to detect damage in metals and composite materials and to assess the significance of the damage with respect to service performance.

Nondestructive Evaluation

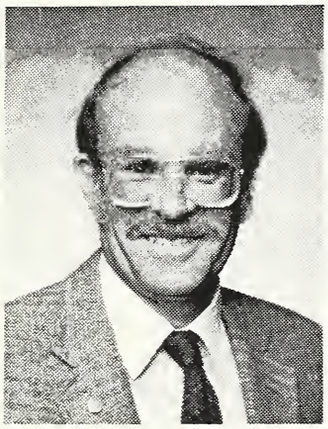

Alfred V. Clark, Jr.
Group Leader

Y. Berlinsky,* D.V. Mitraković,** S.R. Schaps, R.E. Schramm

Our Nondestructive Evaluation (NDE) group develops measurement methods and sensors for evaluating the quality and reliability of materials. We develop NDE techniques to characterize material properties, to detect and size defects, and to measure residual stresses in materials. Our research is transferred to industry for use in intelligent processing and in-service inspection.

Representative accomplishments

- A prototype residual stress measurement system was delivered to the American Association of Railroads for evaluation in their Transportation Test Center.
- A moving sheet device was jointly developed by NIST and Ford Motor Company. It is now in use at NIST to evaluate the feasibility of an on-line ultrasonic system for characterization of steel sheet formability.

---

* Guest researcher from ADA Rafael, Haifa, Israel.
** Guest researcher from the University of Belgrade, Belgrade, Yugoslavia.

Technical Highlights

During FY 91, the NDE Group continued its involvement in technology transfer efforts. A prototype ultrasonic instrument for measurement of residual stress in cast steel wheels was developed and tested. It was delivered to the American Association of Railroads for evaluation at their Transportation Test Center as part of a joint program on wheel safety research.

In a separate project, researchers at NIST and Ford Motor Company jointly developed a device which can move steel sheet specimens at speeds of up to 3 m/s. This simulates the motion of sheet in a continuous annealing line in a steel mill. An array of transducers measures ultrasonic velocity in the material; the ultrasonic velocity is then related to sheet formability.

Ultrasonic Sensor for On-line Measurement of Steel Sheet Formability

Texture, or preferred orientation, has been shown to be a dominant factor in the formability of high quality sheet metal. This material is important in many applications, especially in the production of automobile bodies. The American Iron and Steel Institute (AISI) recently endorsed the concept of intelligent processing of sheet metal formability at a NIST workshop (NIST SP772, 1989). As currently envisioned, the system will be placed in the continuous annealing line where the recrystallization textures are controlled to obtain the desired formability. AISI set certain goals: resolve the formability measure, $\bar{r}$, to an accuracy of ±0.05; make measurements on rapidly moving sheet (speeds of 150 m/min); make system rugged, reliable and cost effective. NIST has tailored its ongoing formability research in FY 91 to meet these goals.

Proof of concept measurements determined that a correlation existed between $\bar{r}$ and $\bar{V}$, the average in-plane velocity of guided waves propagating at three different angles in the sheet. (These measurements also showed a spread of ±0.2 in $\bar{r}$.) We have identified sources of scatter in the data: metallurgical variability and uncertainties in measurements of velocity. The metallurgical variability could arise because thermomechanical processing influences formability. This motivates us to look for correlations based on manufacturer. The velocity measurement uncertainties were attributed to the effects of acoustic wave diffraction, relative velocity in dynamic measurements, and liftoff.

Diffraction: Error analysis shows that we need to resolve velocities to ±0.2% to obtain $\bar{r}$ to ±0.05. Diffraction was a major effect on velocity; the acoustic field spreads out and the wavefronts have curvature. The relation between $\bar{r}$ and $\bar{V}$ is based on "plane wave" theory where the beam is collimated with straight-

straight-crested wave fronts. Thus there is a need to correct the measured arrival times to the arrival times for plane waves. The wavefield generated by the transmitting transducer was measured. This amplitude distribution was used in the diffraction integral which was evaluated to determine phase (and/or arrival time) of the wave. One component is the "plane wave" phase; there are additional terms due to diffraction. By subtracting the latter from the measured arrival times, we correct to the "plane wave" arrival times. These results were found to be in excellent agreement with theory. Figure 1 shows the difference between measured arrival times and "plane wave" arrival time, d/V. Here d = acoustic pathlength; V = phase velocity. The theory was used on data obtained on sheets from 2 manufacturers.

When corrected for diffraction we obtain the results shown in Figure 2. This shows little scatter in correlation curves, for the "S" and for the "K" sheets.

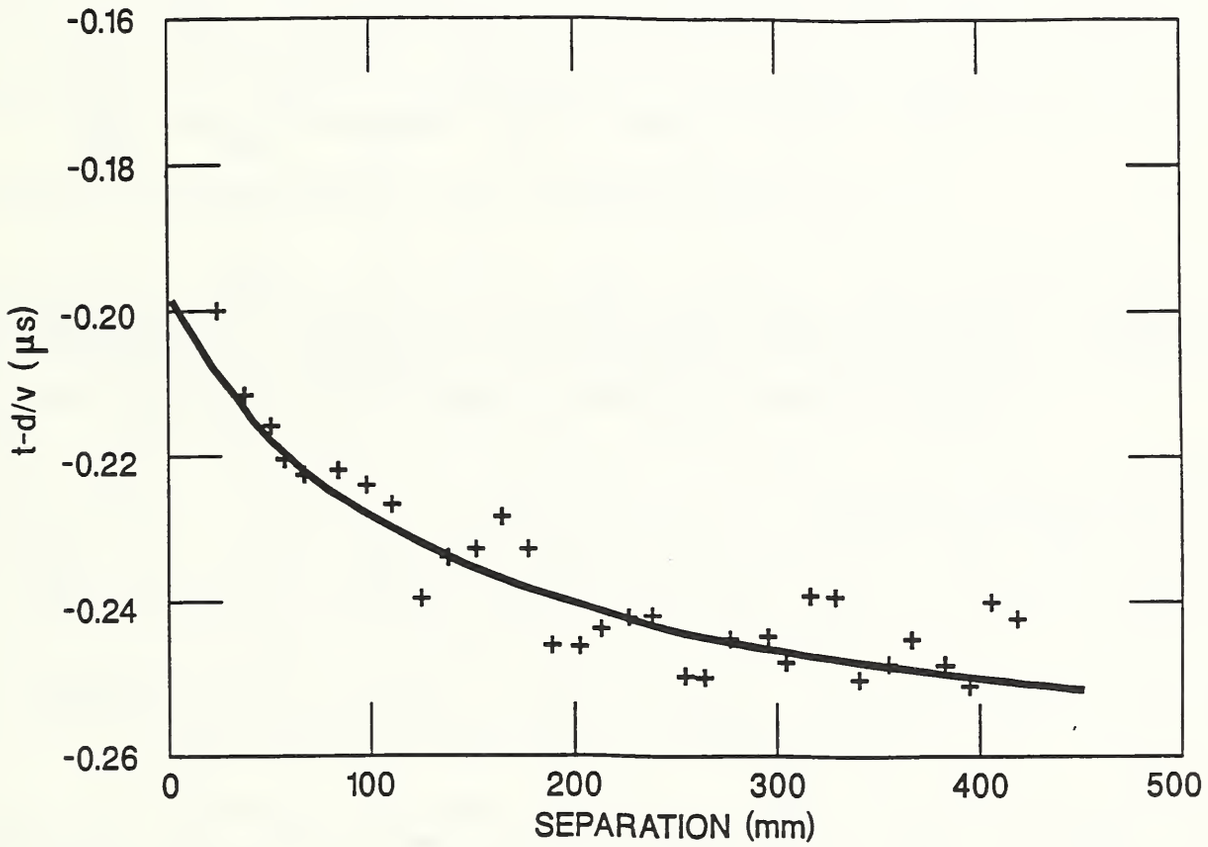

Figure 1. Difference between measured time, t, with diffraction and time, d/V, for a plane wave as a function of transducer separation. The experimental results (+) are compared with predictions of the model [3].

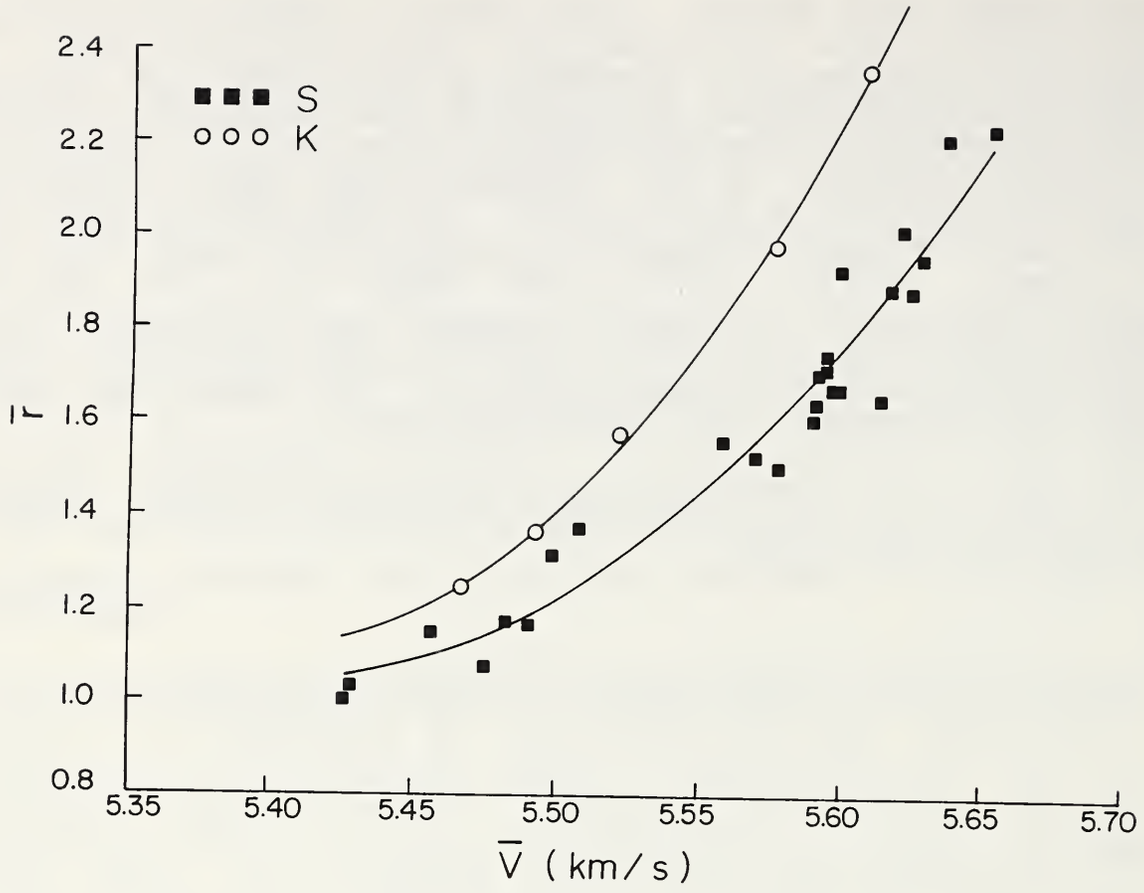

Figure 2. Result of applying diffraction theory to data taken on sheets supplied by two manufacturers (K and S). The $\bar{r}$ values were measured destructively by the manufacturers. The average velocity $\bar{v}$ was measured by NIST.

Dynamic Measurements: We developed a facility for making measurements on rapidly moving sheet as part of a collaboration between NIST and Ford Motor Company. Compressed air enters a cylinder about 7 m in length. This forces a piston down the cylinder. A cable attached to the piston passes over a pulley arrangement and propels a "sled" down a track. A sheet specimen is mounted on the sled and carried under a "bridge" which spans over the track. The bridge houses an array of transducers.

Previous measurements (such as those shown in Figure 2) were made in the static mode. There are several reasons why there could be differences between the static and dynamic mode. For example, when sound is propagated parallel to the direction of sheet motion, the wave arrives sooner than in the static mode, and the wave takes longer when the sound wave is propagated in the opposite direction. We refer to this as the "relative velocity shift" effect.

Liftoff Effects: Another problem of on-line measurements is out-of-plane deflections of the moving sheet, which results in variable clearance (liftoff) between the transducer and the sheet. This causes a phase shift in the velocity measurements. Also, the receiving transducer has an equivalent circuit which consists of an open-circuit voltage source in series with an inductance and resistance. These depend upon clearance between the transducer and the sheet. The effect of changing the circuit reactance is to cause a phase shift, which depends upon liftoff. A change in phase causes a change in the calculated arrival time. We developed a model to predict the phase as a function of liftoff and frequency, with excellent agreement with experiment. We used our model to desensitize the system to liftoff. Tests were done on several steel sheets. When "relative velocity" was accounted for, the difference between the static and dynamic measurements was about 0.02% (1/10 of our error budget).

Control System: The Robotics Systems Division and Materials Reliability Division are now collaborating on development of a control system for intelligent processing of sheet in a continuous annealing line. The processing parameters which must be controlled are being identified. Models of the annealing process will be developed; a control strategy will be selected and implemented using the Real Time Control System developed at NIST.

Ultrasonic Instruments for Railroad Wheel Safety

For several years, the Federal Railroad Administration has funded research to improve railroad wheel safety. On average, there are 33 derailments annually in the U.S., with annual economic loss estimated at $7 million. In addition, there is a significant safety hazard posed by toxic materials being transported by rail.

There are two primary causes of wheel failure leading to derailments: (1) cracks in the wheels, especially those originating in the wheel treads; (2) tensile stresses, which cause growth of cracks and subsequent failure. The NDE Group is developing two separate systems which will detect defective wheels (with tread cracks) and measure the state of stress in the wheels.

Cracked Wheel Inspection: The approach to finding flaws in wheel treads follows the convention of introducing an ultrasonic pulse and listening for an echo return. Figure 3 shows the basic receiver signal. A 20 μs tone burst generates the pulse. This initially overloads the receiver and causes the zero-time spike. The sound takes nearly 1 ms for a round trip around the wheel circumference. Each time it passes the receiver, an electromagnetic acoustic transducer (EMAT) produces a signal indicated by R. In this case, there is a 2 mm deep circular cut in the tread that causes the echoes marked E. While there is only one flaw here, there are multiple acoustic paths. In condemned wheels removed from service there are usually multiple cracks, and the

echo pattern is quite complex. In this instance, the transducer is inside the rail and generates a Rayleigh (surface) wave on the wheel tread as it rolls over the EMAT location; the goal is to make data collection and evaluation completely automatic. Laboratory and limited field testing at the facilities of the Transportation Test Center (TTC) in Pueblo, Colorado, have indicated the workability of the basic idea and operational reliability up to 25 km/h.

Figure 3. Signal from a wheel with an artificial cut 2 mm deep in the tread. R indicates the round trips of the pulse, and E indicates the multiple echoes from the flaw.

Based on the field trials, several improvements have been made to the sensor system: (1) a new coil design suppresses electronic noise, (2) the mechanical system was modified to improve the mechanical reliability of the in-rail EMAT package, and (3) the front end of the amplifier was redesigned to improve the signal-to-noise ratio. The present system is now ready for delivery to TTC for further evaluation. The package includes in-rail transducers, analog electronics to generate and receive the ultrasonic signal, digital electronics to analyze the signal, cabling, and processing software with computer.

Residual Stress Evaluation: Stress fields have a very subtle but measurable effect on the speed of ultrasonic signals. This work measures acoustic birefringence, the change in shear-wave velocity

as the polarization rotates. A shear-wave EMAT, placed on the outside or front face of the wheel tread, sends a pulse through the rim thickness. This reflects from the back face and returns to the EMAT. Timing measurements on this echo are necessary with the polarization along both the radial and hoop directions. The distance traveled in both cases is the same, so we can define the birefringence as the fractional change in velocity or arrival time,

$$B = (t_R - t_\theta) / [(t_R + t_\theta)/2].$$

The effect is small, so typical values are 10^{-3} or 10^{-4}. The stress relationship is

$$B = B_0 + C_A(\sigma_\theta - \sigma_R).$$

C_A is the stress acoustic constant with a value of about -7×10^{-6} MPa^{-1} - indicating again the small size of the stress-acoustic effect. B_0 is the birefringence due to the metallurgical texture; it is of the same order of magnitude as B and competes with the stress effect. The σ's are the directional stresses and σ_R (stress along the radial direction) is usually negligible. The measured value of the hoop stress σ_θ is the average through the entire thickness of the rim.

During the past year, a new measurement apparatus was designed and built. The design includes several features that make the apparatus suitable for field tests: (1) a crossed-coil EMAT that permits the two required measurements to be made without rotating the EMAT was developed , (2) the electronics were improved to permit automated data collection, and (3) a new transducer was developed to allow measurement of near-surface stresses.

The prototype equipment was delivered to the AAR's TTC for field trials. The equipment includes the EMAT, along with the electronics necessary to perform the precision timing, and a fixture to assure accurate positioning on the wheel (Fig. 4). The prototype is part of a major FRA effort to compare our apparatus and approach with those from NASA/AAR and the Central Research Institute of the Polish State Railways. TTC will perform destructive tests on railroad wheels to evaluate the NDE gear.

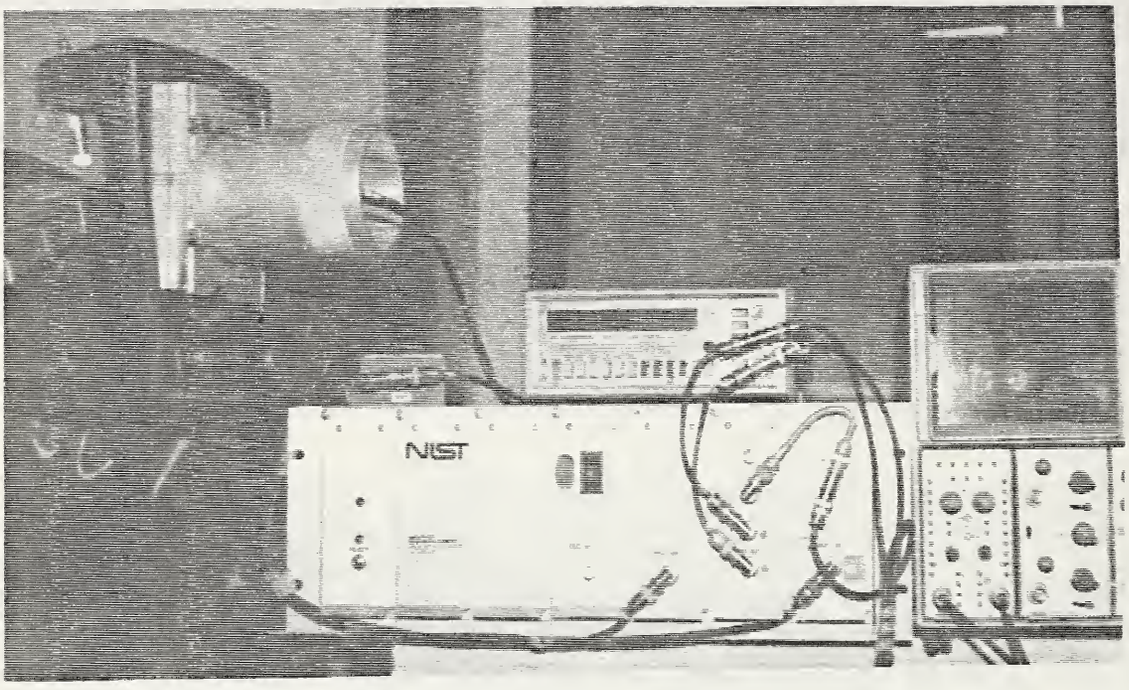

Figure 4. Photograph of the equipment delivered to TTC. To the left, the EMAT is in the cylinder held onto the front face of the wheel rim by the positioning fixture.

Electromagnetic Probes for Characterizing Dielectric Materials

Electromagnetic probes are being developed to characterize the dielectric properties of materials such as the ceramic substrates and FRP printed wiring boards used for electronic packaging. The measurements can be used for process control, for example, characterizing "green state" ceramics prior to the value-added step of sintering. For quality control, measurements can be used to assure consistent dielectric properties in ceramics substrates over the microwave spectrum. We are collaborating with the Electromagnetic Fields Division on research to explore the potential of electromagnetic probes for process control and quality assurance.

Our research focuses on development of a capacitance probe for electrostatic measurements. The Electromagnetic Fields Division is developing an open-circuit coaxial cable for measurements at frequencies up to the gigahertz regime. We share samples and work together on problems posed by industrial firms such as Coors Ceramics, General Motors, and Hewlett Packard.

Manufacturing of ceramic substrates used in electronic packaging can be improved by measuring the green state ceramic material density and adjusting the compaction during manufacturing. A low

frequency capacitive probe was built and used to test green state ceramic samples to evaluate it as a sensor of density for use in process control. The test results indicate that this probe can measure density to better than 0.2% on samples with alumina densities in the 50% to 60% range.

The probe, shown in Figure 5, operates by generating an electric field between its outer electrodes. As this field travels above the probe surface, it passes through the sample. The inner electrodes detect this electric field and variations in this field caused by sample properties such as permittivity. Since permittivity is a function of green state density, the probe effectively measures sample density.

The capacitance probe has also been useful for moisture sensing and liftoff measurements. For General Motors, we demonstrated that potential for sensing the moisture content of green sand used for foundry operations. The liftoff sensitivity is being used to improve ultrasonic formability measurements under on-line conditions where liftoff may vary.

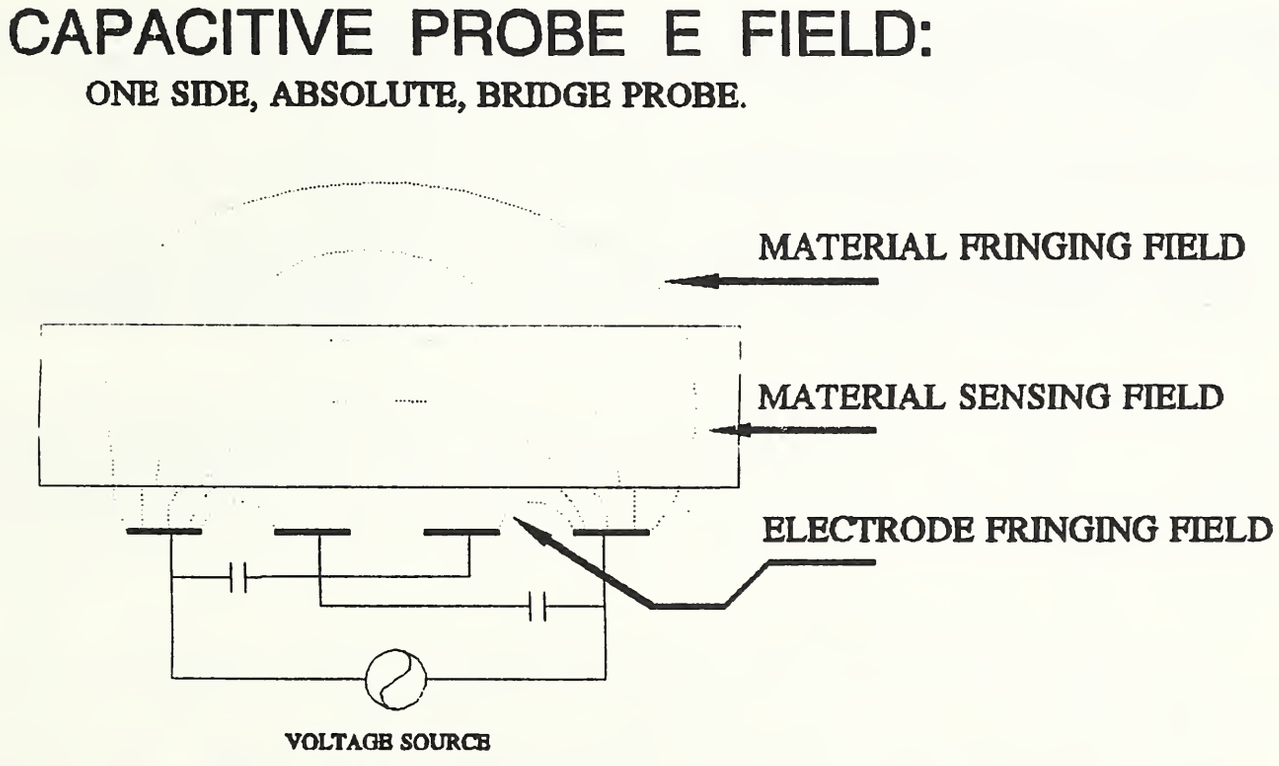

Figure 5. Capacitance probe for one-sided measurements.

Nondestructive Evaluation of Composite Materials

Christopher M. Fortunko
Research Leader

D.W. Fitting, V. K. Tewary*, L.J. Bond**, E. Jensen+, and M. Renken++

Our research in nondestructive evaluation (NDE) of composite materials is aimed at improved experimental methods for material-property characterization and flaw detection and sizing. In addition to a considerable experimental and special instrumentation-development activity, we are also developing theoretical models and computer-visualization aids, which are needed to establish model-based material-property and flaw-characterization procedures. The Composites-NDE technical program also includes a broad range of university, other government agency, and industrial interactions.

Representative Accomplishments

- A high-pressure, gas-coupled acoustic microscope was designed, built, and demonstrated. Proof-of-concept experiments on silicon wafers showed excellent signal-to-noise ratio and resolution potential below 10 μm.

- An acoustic array consisting of a high-power, broad bandwidth point source and a linear array of high sensitivity point receivers has been designed and built. The initial experiments demonstrated excellent signal-to-noise ratio in thick glass/epoxy composites.

---

* Visiting Scientist from Ohio State University, Columbus, Ohio.
** NIST-supported Research Professor at University of Colorado at Boulder.
+ Co-op Student from Colorado School of Mines, Golden, Colorado.
++ Co-op Student from Valparaiso University, Valparaiso, Indiana.

Absolute Measurements of Elastic-Wave Phase and Group Velocities in Lossy Materials

Ultrasonic NDE methods are used to insure that composite materials are fit for their intended application. Although flaw detection is certainly important, the real measurement challenges exist in the area of material-property characterization. Specifically, a particular interest is quantifying material attributes including: fiber volume fraction, fiber orientation and length distributions, porosity content, quality of bonding between the matrix and reinforcing materials, and others. Elastic-wave velocities appear to be especially useful as discriminants of attributes such as fiber volume fraction and porosity content. Absolute phase velocities are of special interest, since they are needed to determine the elastic moduli.

In low-loss materials, the phase-velocities of megahertz elastic waves can usually be determined using traditional Fourier or Hilbert spectroscopic methods. Group velocities can be determined using pulse-echo-overlap and similar methods. However, such methods are inadequate in many thick-section materials that exhibit high, frequency-dependent propagation losses. Generally, materials which exhibit propagation-loss variations in excess of 30 dB across the passband of the transducer belong to this category.

We have addressed the problem by designing new measurement hardware and signal-processing algorithms. Our method is mechanized as a pulsed, swept-frequency interferometer. The accuracy and reliability of the method are enhanced by a combination of circuit-design improvements, which increase the signal-to-noise ratio and linearity, and signal-processing methods, which effectively remove circuit-related measurement errors and compensate for diffraction. Currently, we are able to make measurements in the 50 kHz to 5 MHz frequency region in thick materials that exhibit propagation losses up to 100 dB across the passband of the transducer.

To illustrate the method, we determine the phase velocities in a very lossy, 50 mm thick, glass/epoxy specimen in the 0.3-1.2 MHz region. Figure 6 shows a block diagram of our measurement configuration. Significantly, the configuration of Figure 6 uses the same transducer to transmit and receive the probing ultrasonic signals. This "pulse-echo" configuration is needed to address many practical problems where access is limited to only one side.

To improve the system dynamic range and frequency selectivity, our phase-sensitive receiver is implemented as a superheterodyne receiver equipped with a two-channel, synchronous demodulator. Each channel of the demodulator is implemented using a double-balanced mixer followed by a gated integrator.

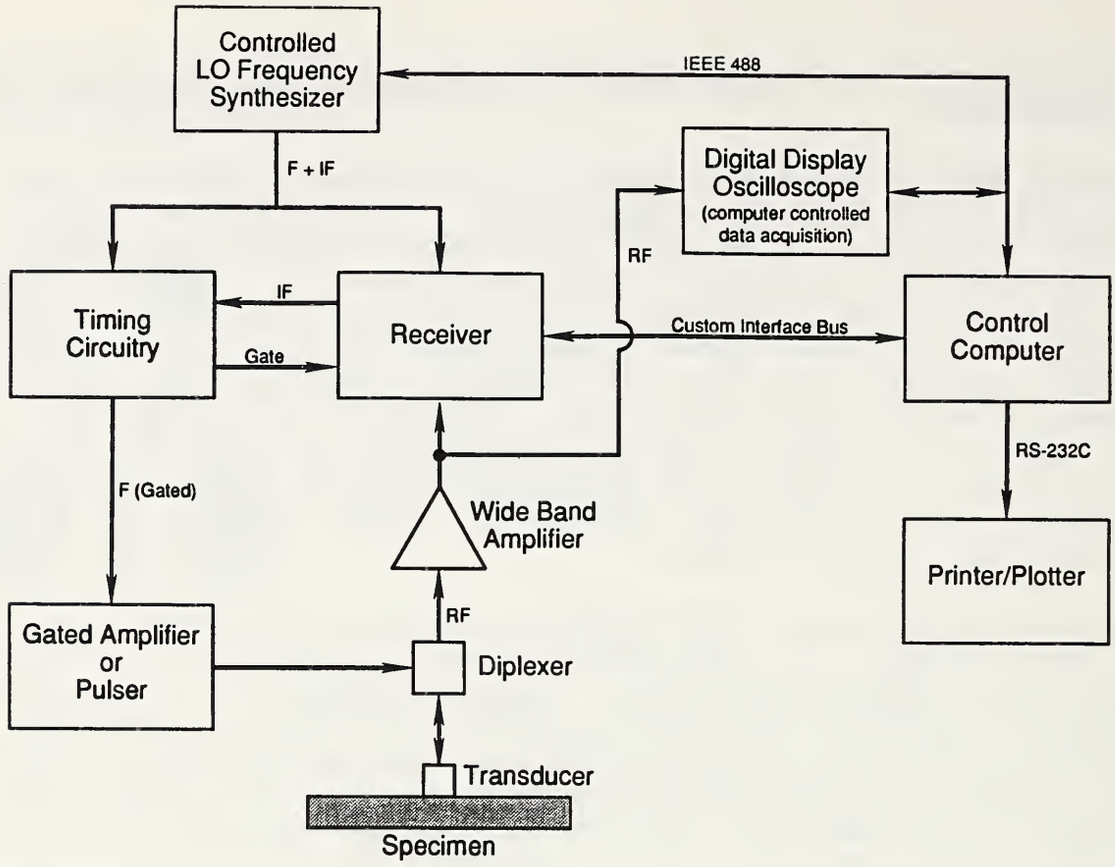

Figure 6. Block diagram of experimental configuration.

We selected a wet-filament-wound specimen, because it was known to exhibit large, frequency-dependent propagation losses as well as variations in the fiber/resin ratio. The large, frequency-dependent propagation losses resulted from the entrapment of small amounts of air in the matrix of the material during the winding process. The variations in the fiber/resin ratio were caused by another characteristic of the fabrication procedures.

Figure 7 shows the phase of the received signal as a function of frequency in two different regions of the same specimen: a resin-rich and a resin-poor region. The data were corrected for the effects of: diffraction, phase shifts through the electronics and transducers, radio-frequency leakage, and others. Ultrasonic velocity measurements effectively discriminated material properties. In the first region, the fiber/resin ratio and pore content were 57% and 2.9% by volume, respectively. In the second region, the fiber/resin ratio and pore content were 66% and 0.7%. In the first region, the phase velocity is 2880 m/s. In the second region, the velocity is 3310 m/s. In addition, in the first region the phase velocity exhibits dispersive behavior. We attribute this to the greater pore content.

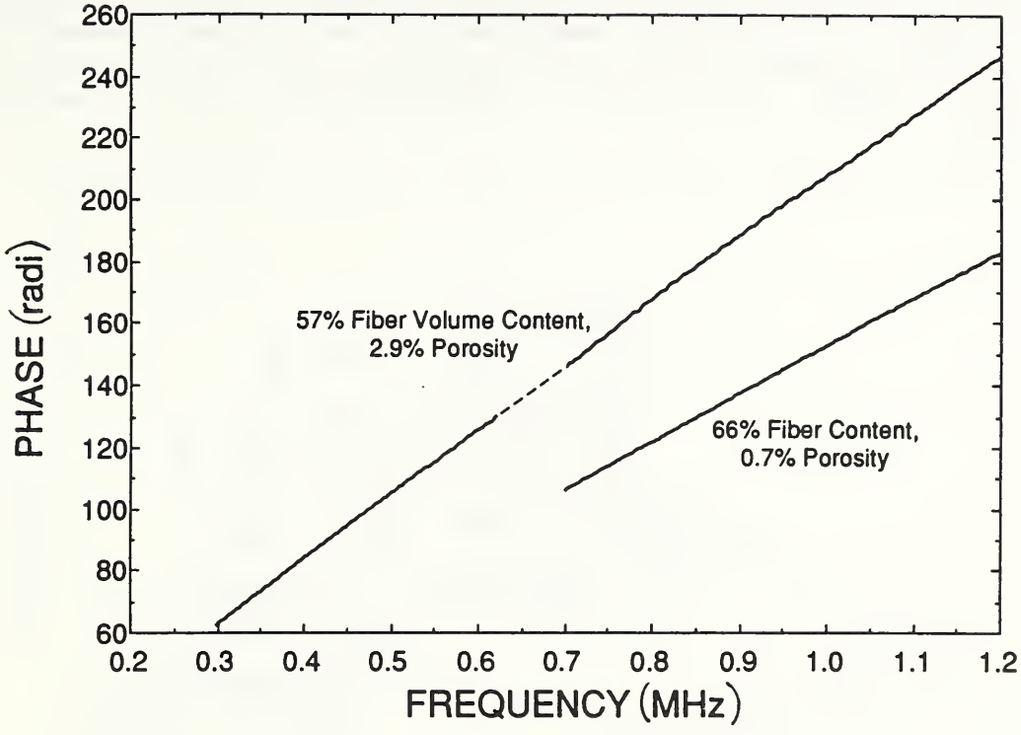

Figure 7. Corrected phase for two locations from wet-filament wound glass/epoxy composite.

Gas-Coupled Transmission Acoustic Microscopy

The technology for high pressure gas-coupled transmission scanning acoustic microscopy has now been demonstrated. A system working from 10 to 30 MHz at pressures up to 10 MPa (100 bar) and room temperature (15 to 25°C) has been developed. It has been used to measure the absorption and velocity of ultrasound in air and argon under a range of conditions. It has then been used to demonstrate the feasibility of a transmission scanning acoustic microscope with measurements through a silicon wafer, and this has been achieved with good signal-to-noise ratio.

The system consists of a cylindrical thick-walled pressure vessel with external dimensions approximately 1 m long and 40 cm in diameter. The measurement stage which goes inside the vessel is shown in Figure 8. The transmitter used to measure gas properties is an 8 mm diameter lithium niobate (Y-cut, rotated 36°) crystal set onto a fused-quartz buffer rod 50 mm long and 25 mm in diameter. The transmitter is excited using a gated tone burst with a 200 V peak signal, typically 10 to 20 cycles long. The receiver is similar to the transmitter, but the buffer rod is 40 mm long. The received signals are passed through manually controlled

attenuators with 132 dB overall dynamic range and 1 dB resolution. The signals are then amplified in a broadband receiver with a 76 dB dynamic range. Transducer separation is varied under computer control and measurements of the absorption were made at a series of frequencies under different combinations of pressure and temperature.

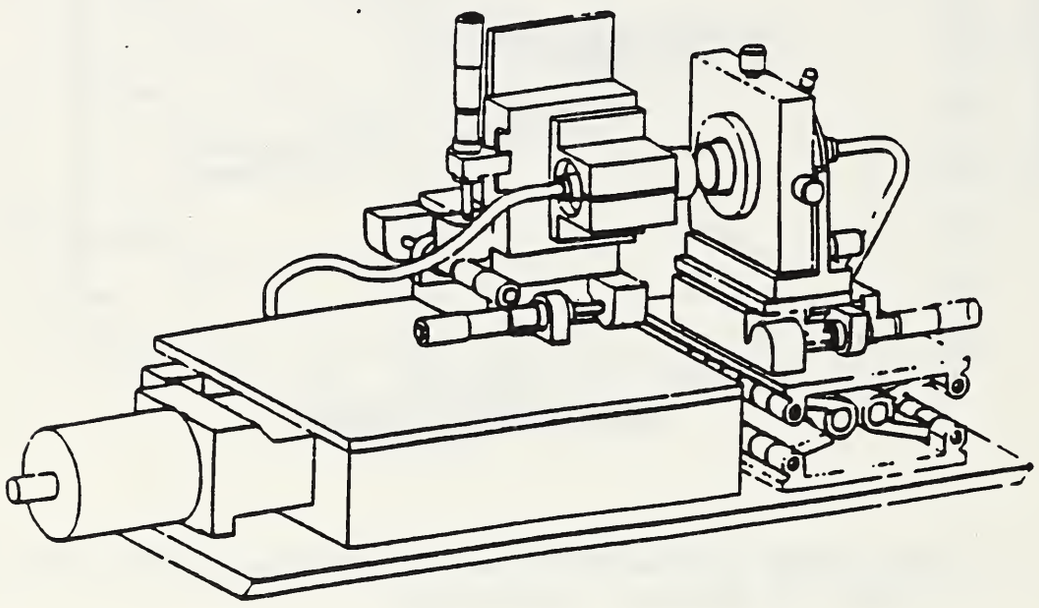

Figure 8. Mechanical transducer manipulation stage.

Data obtained for the absorption in argon are shown in Figure 9. These data are in close agreement with that predicted for small amplitude waves in an ideal gas. When the pressure is greater than about 3 MPa (30 bar) it is necessary to consider the gas as non-ideal. The recent results have demonstrated that a wide range of high frequency (greater than 5 MHz) gas-coupled ultrasonic non-contract measurements for material characterization and inspection, using inert gases are now known to be practical. Applications include process control, electronic semi-conductors and electronic packaging, green state ceramics, compacted powders, coatings, thin films, and magnetic tape.

Two additional steps are necessary to operate the prototype system as a scanning acoustic microscope (SAM). First, we must obtain and install focused transducers with acoustic-matching layers. With existing electronics, this would enable measurements in the 10–30 MHz range. Second, a sample manipulation stage must be installed for scanning operation. These items will be integrated into the system in 1992. After demonstrating SAM capabilities, the resolution limits will be explored. The potential exists for gas-

coupled measurements up to at least 200 MHz, which in gas gives resolutions equal to that achieved with a 1 GHz water-coupled system (such systems use ultrasound with about 1.5 μm wavelength).

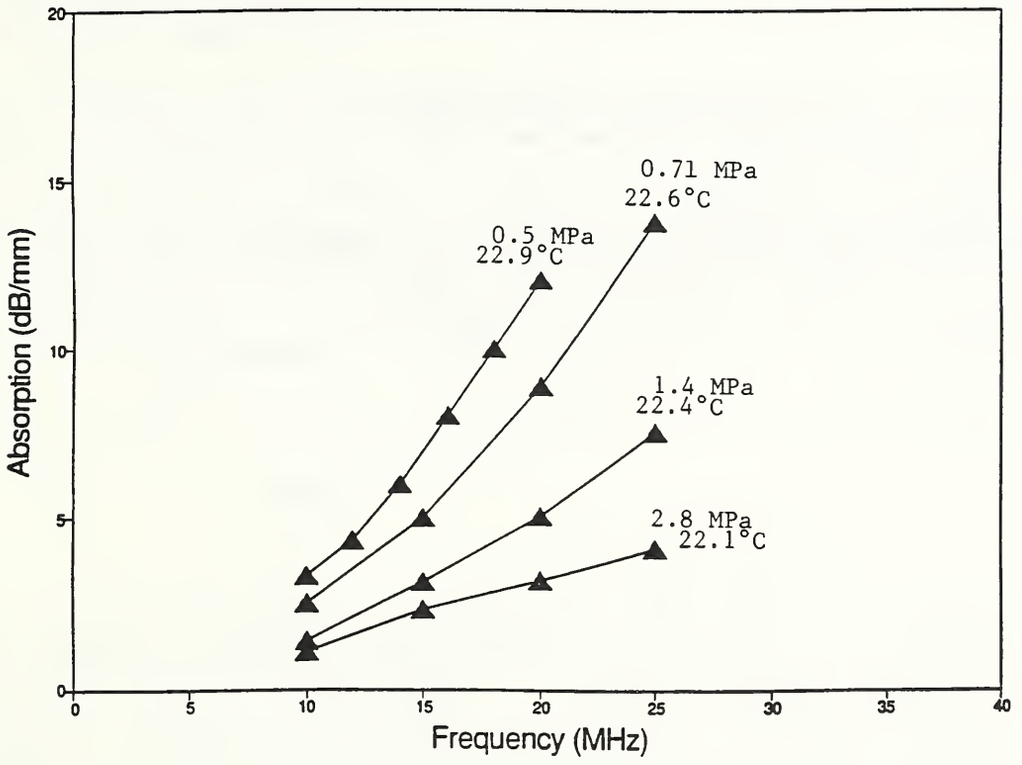

Figure 9. Measured values for absorption in argon.

Flexible Sensor Array System for Monitoring the Long-Term Service Performance of Thick Composites

An ultrasonic sensor array system is under development for in-service inspection of thick polymer composite structures. The inspection concept (Figure 10) for the system is based on "reflection seismology", which has proven quite successful for determining subsurface structure of the earth. A number of spatially-separated, high-power, wide directivity point sources broadcast an ultrasound field into the composite. Scattering and reflections from internal structures, which return to the surface, are sampled by a dense linear array of point receivers. The receiving array signals can be processed in a number of ways to produce both cross-sectional images of the material or to yield quantitative material properties along a "line-of-sight" through the composite.

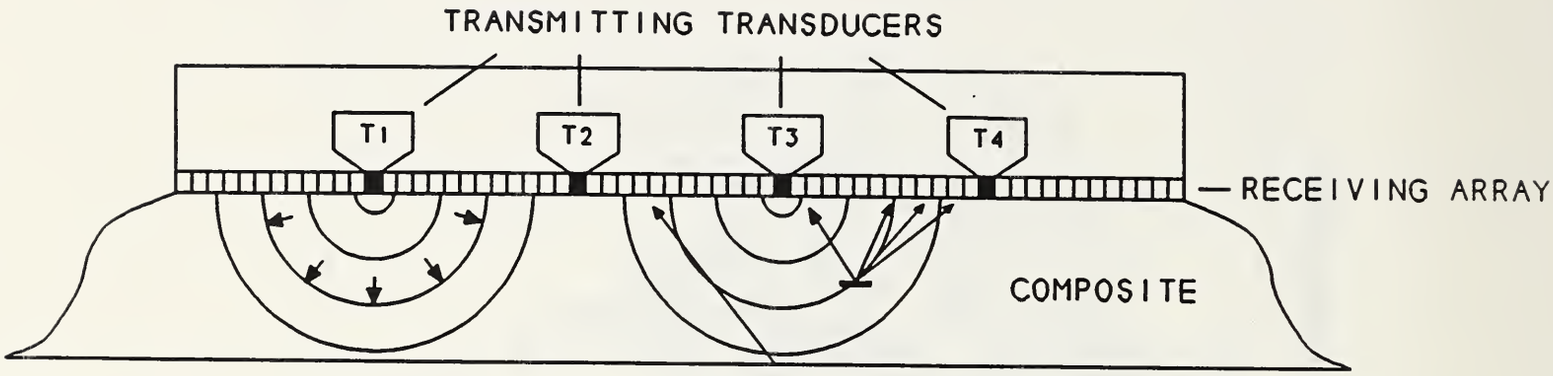

Figure 10. Concept of multiple transmitters and a linear array capable of acquiring broadband ultrasonic pulses over a large angular range. The array can be used for obtaining high-resolution images, detecting in-plane damage such as delaminations, and out-out-of-plane damage including cracks. In addition, the broadband nature of the pulses permits collection of data related to material properties which vary as a function of depth.

In our inspection approach, the linear array is needed primarily to increase the sensitivity to low-contrast, in-plane features and out-of-plane cracks. The sensor array (transmitters and receiving elements) will be coupled to the composite by a flexible, dry-coupling medium. Processing the array signals is performed by fast digital computing hardware to yield a high-resolution "B-scan" type image of the material.

The advantages of the reflection seismology approach to inspection of thick polymer composites include the ability to deal with anisotropy and inhomogeneity, capability of rejecting coherent noise, enhanced sensitivity to low-acoustic-contrast material anomalies, decrease in background speckle of the images and an ability to cope with regional loss of array-to-structure coupling or nonfunctional receiving elements.

The enabling technologies for the inspection system are point sources, an array of point receivers, wide-dynamic range signal

acquisition and algorithms for imaging and materials characterization. Under DARPA sponsorship, we have designed, fabricated and tested components for the three major subsystems of the inspection system - sensor array, pulser module and instrumentation module. NIST collaborators in Gaithersburg have developed an adaptive algorithm for processing the sensor array data to produce high-resolution images even in a significantly inhomogeneous composite.

Figure 11 shows the experimental arrangement of transmitter and receivers for acquisition of "reflection seismology" data from a polymer test block with a single point scatterer embedded at a depth of 25 mm. The common-source data set acquired with the point source and array receiver is shown as a plot of receiving element signal as a function of time for each of the 32 elements in this particular array. Similar high signal-to-noise ratio data have also been achieved on thick (46 mm) glass/epoxy composites.

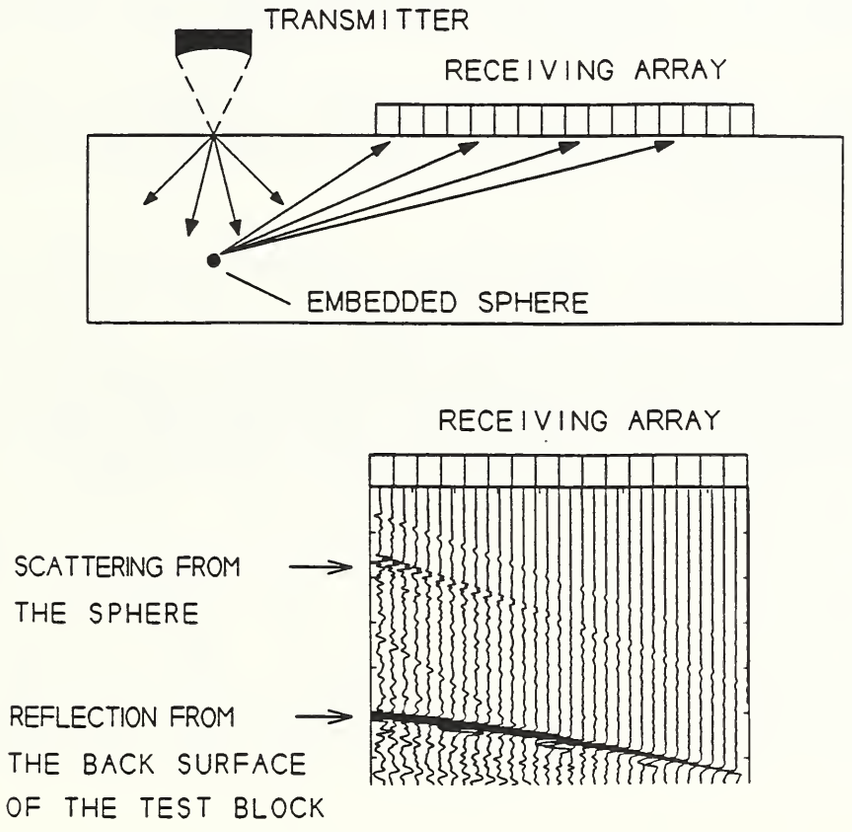

Figure 11. Configuration of point source transmitter and linear array of point receivers for acquisition of scattering data. The waveforms acquired by the receiving array are displayed. A direct wave, scattering from the sphere and a reflection from the bottom (75 mm deep) of the test block are discernable.

Propagation Scattering of Elastic Waves in Anisotropic Solids

The propagation and scattering of elastic waves provide a valuable tool for the quantitative nondestructive evaluation of composite materials. Because, in general, composite materials are highly anisotropic, it is important to develop theoretical methods for the calculation of wave propagation characteristics in anisotropic media.

A time-dependent three-dimensional Green's function method has been developed to study the propagation of elastic waves in a general anisotropic solid. A new closed-form representation is obtained which is the exact solution of the Christoffel wave equation for anisotropic solids. The new representation is numerically more efficient than the traditional representations based on the use of Fourier and Laplace transforms. The retarded Green's functions are derived for an infinite anisotropic solid and an anisotropic half-space with the new representation. The method is applied to calculate the elastic-wave response of an anisotropic cubic solid to highly localized delta function and step function-type pulses. The method will now be applied to less symmetric solids.

The results of the Green's function modelling are being used as an aid in defining spatial and time domain transducer responses that maximize the detection reliability for specific flaw categories and material anisotropies.

To test the validity of the newly developed theoretical model we have designed a unique experimental test fixture for mapping the wavefields produced in an anisotropic solid. Measurement of the ultrasonic wavefield in a solid from receiver scans on flat plates requires corrections to be applied and also limits the angles over which measurements can be made. We have designed and fabricated a measurement apparatus to overcome these limitations. An ultrasound source is coupled to the flat portion of a hemisphere or half-cylinder of the composite. The instrument we have fabricated is shown in Figure 12. The C-arm (Flag 3) scans a miniature, wide bandwidth receiving transducer over the specimen (polar angle scan). Rotating the specimen with the rotary stage (Flag 11) permits changing the azimuthal angle. The advantages of the fixture are that the ultrasonic path length is equal for all angles and measurements may be made over a wide range of angles (>±85°).

SOURCE TEST FIXTURE

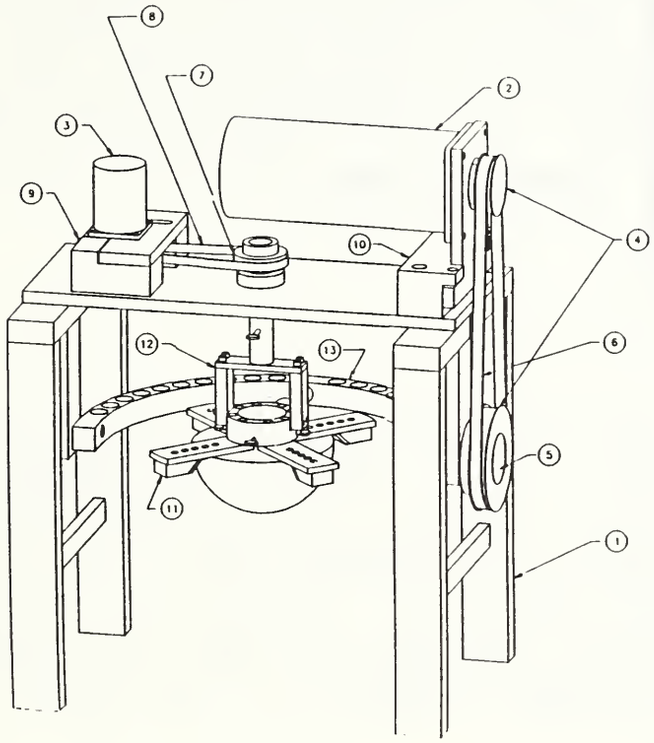

Figure 12. Fixture for mapping the ultrasound wavefield generated in a composite. The specimen is machined into a hemisphere or a half-cylinder for these measurements.

Fracture

David T. Read
Research Leader

J.R. Berger,* I.-H. Lin, M. Szanto,** V.K. Tewary,+ R.M. Thomson, S. Yukawa

Our research in the mechanics and physics of fracture emphasizes advanced materials such as composite materials and electronic-packaging materials. In addition, we continue to study the fracture behavior of steels. In the case of composites, we are interested in damage mechanisms which are local events that deteriorate the strength and stiffness of composites but do not necessarily trigger fracture. For electronic packaging, we are starting to develop experimental and analytical techniques for characterizing fracture behavior in thin films and multilayered materials.

Representative accomplishments

- A micromechanical test apparatus was assembled and used for in-situ measurements of the strength and ductility of aluminum thin films deposited on a silicon substrate.

- The stress intensity factor for an interfacial crack at the interface of two dissimilar thin films has been derived for the mode-III case.

- A powerful method for solving the Hilbert problem has been developed by using an orthogonal complex transform. This enables us to use Green's functions to solve a number of fracture problems for composite materials.

---

* Until June 1991; currently at Notre Dame University.
** Guest researcher from the Nuclear Research Center, Negev, Israel.
+ Visiting scientist from Ohio State University, Columbus, Ohio.

Mechanical Property Measurements on Thin Films

The concept of the "testing machine on a chip" has been proved workable: We have carried out tensile tests of arrays of four TiAlTi trilayer specimens. Using four specimens instead of one increased the available load and decreased the signal-to-noise ratio in the load signal. Each individual specimen was 1000 x 250 x 1 μm. The total load measured in this tensile test was approximately 0.4 N. The total displacement was about 10 μm. The load-displacement data are displayed as a stress-strain curve in Figure 13. Average stress and strain are plotted. Because one specimen broke before the other three, the curve has two branches at high strains.

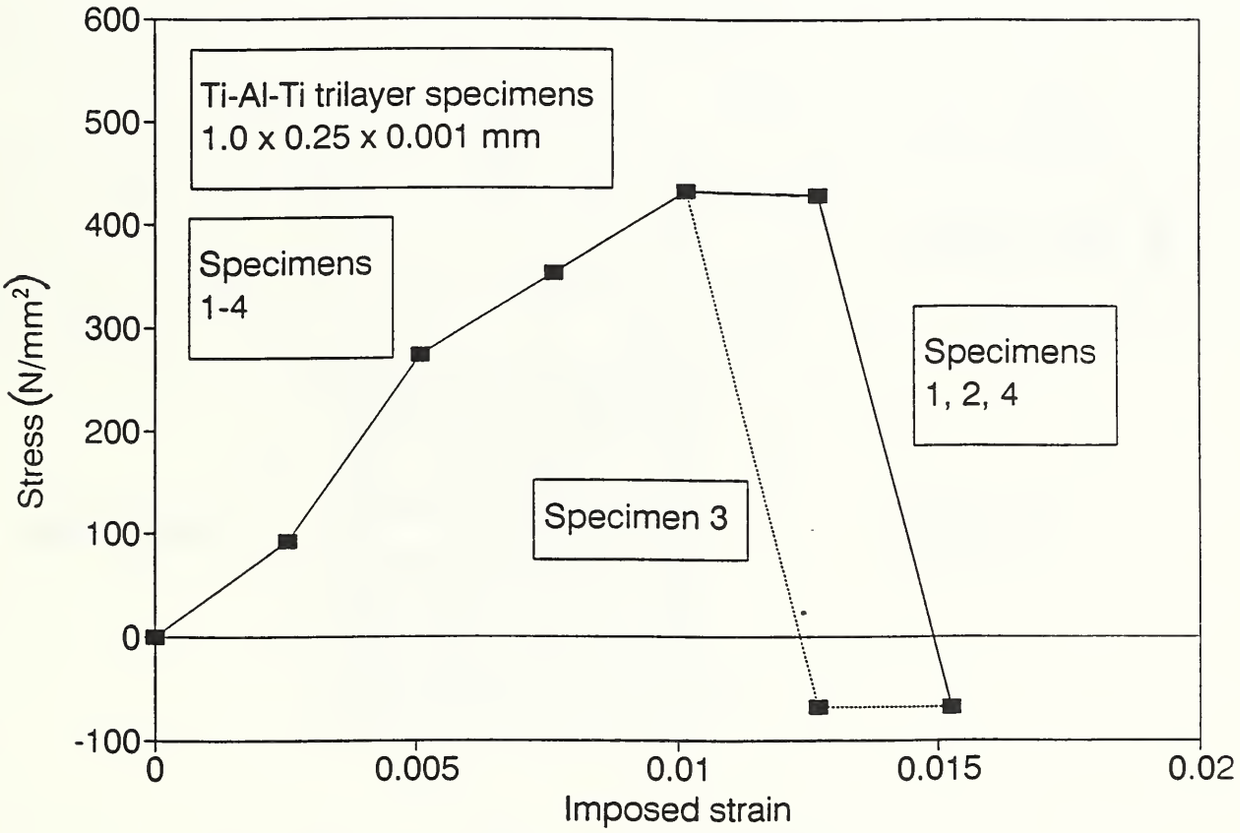

Figure 13. Stress-strain behavior of an aluminum-titanium thin film. The averaged behavior of four parallel specimens is shown.

Successful fabrication of the thin film specimens on the compliant silicon test frame required a series of careful processing steps. Important advances were the use of plasma cleaning of the silicon immediately before evaporating the specimen films, alignment of the pattern for the compliant silicon frame on the back side of the wafer to the specimen pattern on the front of the wafer by using a mask aligner equipped with an infrared microscope capable of seeing through silicon, and designing the compliance of the silicon structure to be neither too low, which makes testing the thin film specimens impossible, nor too high, which allows the specimens to fail prematurely. The design of the successful compliant silicon frame is shown in Figure 14. The specimen is suspended between the two stems in the center of the structure. A piezoresistive load cell fabricated into one load stem is connected by metal thin film traces to pads on a header, where the power can be introduced and the signals extracted using wafer probes.

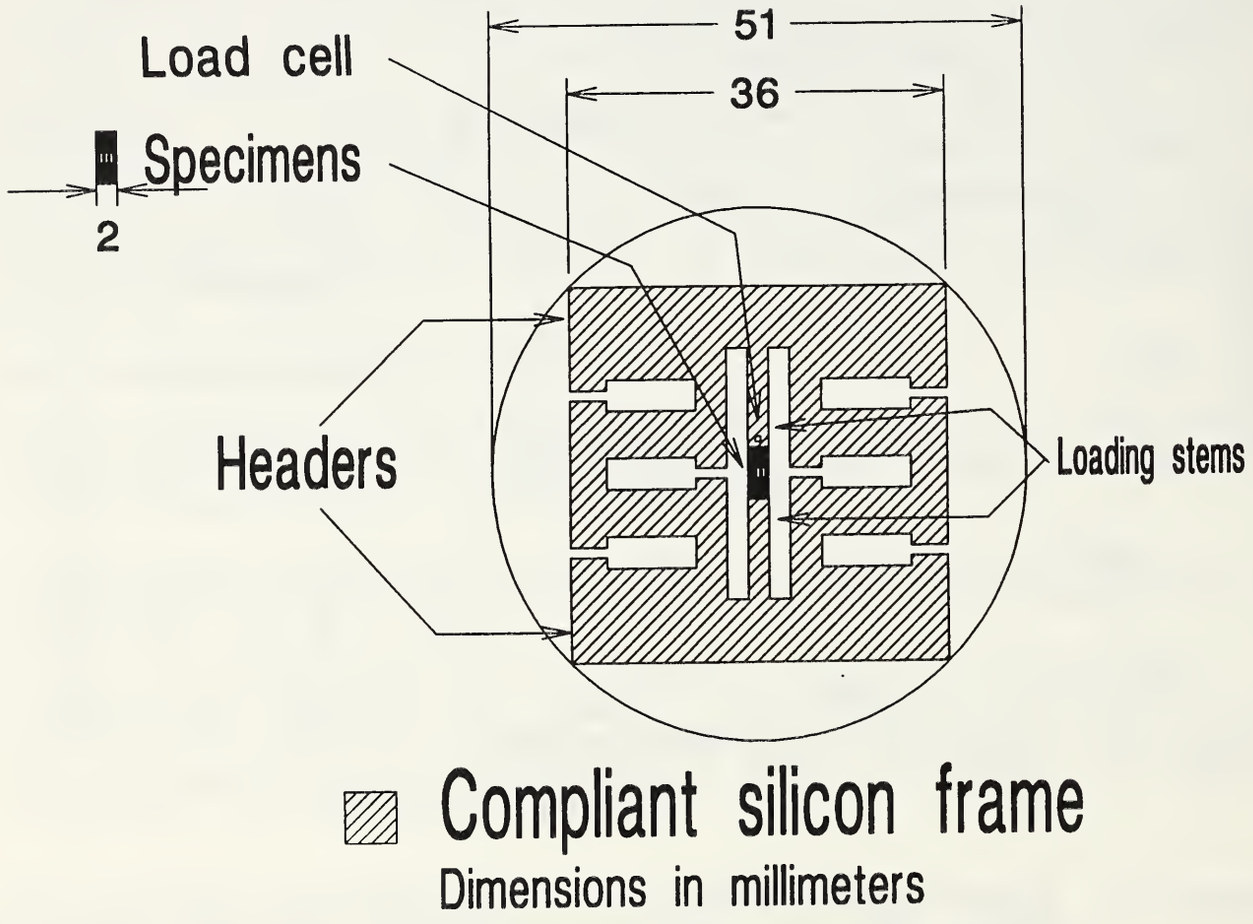

Figure 14. The compliant silicon frame for testing thin film specimens is etched out of a 51-mm-diameter silicon wafer.

Improvements are needed in the load and displacement sensitivity of the test assembly. Preliminary results from the first few tests show that the elongation-to-failure of the present specimens is lower than would be expected for bulk materials. The measured elongation-to-failure was about 1 percent, while bulk aluminum often reaches 20 percent. The cause of this behavior has not yet been determined; details of the specimen preparation procedure may have influenced the result. The observed strength and Young's modulus were not distinguishable from the normal range of values, but the error bounds in these quantities need improvement.

Fitness-for-Purpose Assessment of Solder Joints

An important failure mode in solder joints is low-cycle fatigue. Fatigue in structures occurs preferentially at sites of geometric strain concentration. To facilitate finite element analysis, we have developed a computational procedure which utilizes the J-integral to evaluate the stress and strain at the root of a stress concentration. The applied J-integral is insensitive to mesh refinement, to the exact shape of the mesh at the notch root, and to plastic flow at the notch root. The applied J-integral and the radius-of-curvature of the notch root are sufficient to determine the stress and strain at the notch root, where one component of the stress is much larger than all the others. Figure 15 displays results for a deep single-edge notch in Pb–Sn 60-40 solder. The profound effect of the notch-root radius on the notch-root strain is clear. The strains at the notch root are plastic over practically all of this plot.

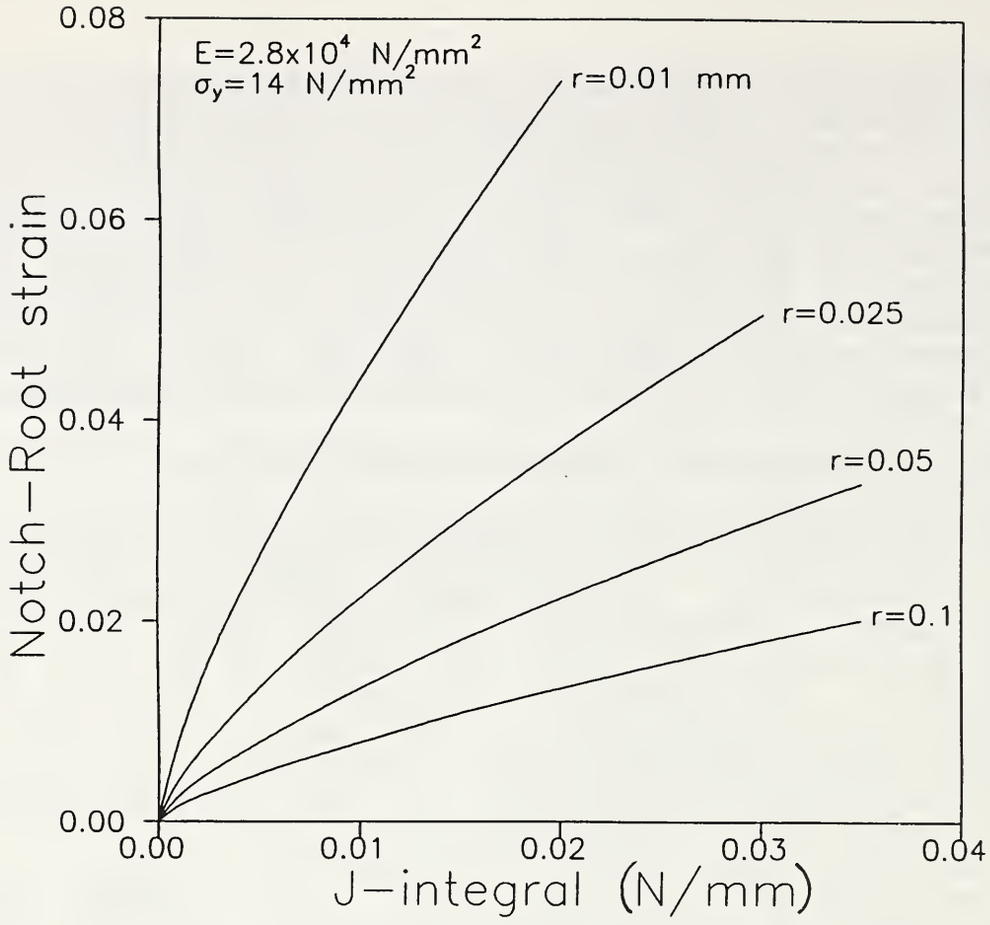

Figure 15. Calculated notch-root strain as a function of applied J-integral and notch-root radius for a single-edge-notched specimen of PbSn 60-40 solder.

Finite element analysis of solder joints requires input data on geometry, imposed loads, and material properties; it produces output data on the J-integral values at cracks and notches and on stress and strain. But it requires considerable effort. If the overall stresses and strains are estimated from the imposed loads, and if the J-integral is approximated from the overall strains, then the results of the finite element analysis can be approximated. This approximation may be more in keeping with the quality of the input data than a full finite element analysis.

Based on these considerations, a two-level fitness-for-service assessment procedure for solder joints has been proposed. The higher (second) level is the full finite element analysis method, using automatically generated meshes. The first level takes as input the imposed loads, the average size of the solder joint, and the radius of curvature and the orientation of the notch roots. The J-integral is estimated from the overall strains and the notch depth; the strain at the notch root is evaluated using the J-integral and the radius of curvature. The fatigue life of the solder joint is evaluated using literature fatigue data. This first-level assessment could be sufficient in itself, or it could

show whether, in a specific case, there is a need for a full finite element analysis.

Elastic Green's Function for Fracture Mechanics of Composite Materials

The elastic Green's function provides a convenient mathematical tool for the stress analysis of solids. However, calculation of the Green's function for anisotropic solids usually involves solving an inhomogeneous vector Hilbert problem. We have developed a powerful method for solving the Hilbert problem by using an orthogonal complex transform. This method is particularly convenient for application to anisotropic composite materials containing cracks and/or free surfaces.

We have applied this method to calculate the displacement and the stress fields in an anisotropic Cu/Ni composite containing an interfacial crack, subjected to uniform normal and shear loading. We have also investigated in great detail the effect of a free surface in an anisotropic bimaterial composite. In particular, we have studied the effect of a free surface in (1) stainless steel containing an Σ-5 grain boundary, subjected to plane strain as well as generalized plane strain, and (2) graphite/epoxy composites of the types (0/90), (45/-45), and (30/-30) subjected to generalized plane strain.

The calculated stress field for a shear loaded Cu/Ni composite containing an interfacial crack shows that the stress field is oscillatory, but, except very near the crack tip, the oscillations are negligible. This is an agreement with the earlier predictions of other authors which were mostly based upon isotropic models.

The effect of a free surface in a composite is to introduce singularities in the stress. This free edge effect is important in the analysis of delamination failure of the composites. Our calculations provide a comprehensive study of these singularities. In addition to the singularities, we find that, in certain cases, the stress field may also contain an oscillatory factor, similar to that for an interfacial crack.

Cleavage, Dislocation Emission, and Shielding for Interfacial Cracks in Bimaterials

The conditions for the existence of a cleavage interfacial crack in a bimaterial and its response to all types of external loads when shielded by neighboring dislocations were considered. Results were obtained and summarized into three parts: (1) general relations are derived for the elastic interactions between a cleavage interfacial crack and a dislocation and between pairs of dislocations in the presence of the crack in a bimaterial. These results are expressed in terms of the local k-field of the crack tip, the shielding contributions from the dislocations, and the

complete specification of the forces on the two types of defects; (2) dislocation emission depends on the full specification of all three components of the local k-field. The primary result is that combined cleavage and emission states are possible under mixed loading wherein a cleavage crack can generate significant plasticity in mode II and mode III dislocation configurations into the soft medium in a bimaterial; (3) the overall static equilibrium configuration of the shielded core crack and its dislocation cloud is considered. General theorems developed show that for symmetrical dislocation configurations, mode I configurations only shield the k_I loading at the crack tip, and the slip force mutually exerted on two symmetrically placed dislocations is exactly zero. Simplified fracture toughness relations were also derived.

Interfacial Crack in Thin Film Composites

Dislocation modelling of a center interfacial crack in thin film composites was studied for a mode III antiplane shear loading. The Hilbert integral equation was solved for the dislocation density function, which is found as nonsymmetrical inside the center crack when the ratio between the thin film thickness and the crack length is finite. The crack tip extension force G is expressed as a function of the dissimilar elastic constants μ associated with the thin film bicrystals and the size ratio between the thin film thickness a and the crack length l:

$$G = G_o F(\mu_2/\mu_1) F(l/a)$$

$G_o = K^2(o)/2\mu$ and K(0) is the stress intensity factor for the infinite thin film.

PROPERTIES

The Cryogenic Materials and Physical Properties Groups investigate the behavior of materials at low temperature and measure and model the properties of advanced materials, including structural alloys, conductors, composites, ceramics, polymer resins, and superconductors.

Cryogenic Materials

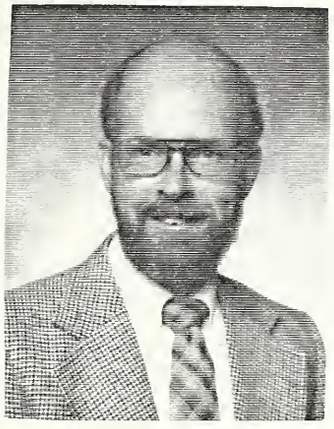

Harry I. McHenry
Acting Group Leader

A. Bussiba*, E.S. Drexler, J.D. McColskey, P.T. Purtscher, R.P. Reed**, N.J. Simon, R.L. Tobler, and R.P. Walsh

We study the mechanical, physical, and metallurgical properties of materials in the temperature range from room temperature down to 4 K. Goals of our research are the characterization and development of metals, alloys, polymers, and composites; the development of testing procedures and standards; and the collection and evaluation of material property data.

Three major programs were funded by other agencies during the past year: (1) the Department of Energy continued to sponsor the development of materials technology to design and build superconducting magnets for fusion-energy systems; (2) the Air Force sponsored a program to evaluate aluminum-lithium alloys for cryogenic tankage in the Advanced Launch System; and (3) the Department of Defense sponsored a program to evaluate materials for Superconducting Magnetic Energy Storage. We have expertise in and unique facilities for measuring tensile, fracture, impact, shear, creep, and fatigue properties at very low temperatures. Our measurements contribute to design and safety assessments, and we consult on material selection and properties for a wide range of cryogenic projects.

---

* Guest researcher from the Nuclear Research Center, Negev, Israel.

** Consultant to NIST.

Representative Accomplishments

- Two austenitic stainless steels and a nickel-base superalloy were evaluated at 4 K for use in the superconducting cable conduit sheath being developed for the International Toroidal Experimental Reactor.

- Two of NIST's proposed test standards for structural alloys covering tension and impact testing at cryogenic temperatures were approved by ASTM.

- A new compression–shear test for composites was proposed, developed, and used to evaluate insulating materials for superconducting magnets.

Advanced Structural Alloys Evaluations

Aluminum-lithium alloys now commercially available offer higher stiffness and strength-to-weight ratios than conventional aluminum alloys and are contenders for aerospace applications. Last year's cooperative program with NASA demonstrated that these alloys are oxygen compatible for use in the cryogenic tankage of the Advanced Launch System. This year, to contribute to structural reliability assessments, we tested commercial 2090 and x2095 alloys using 100-mm wide surface-cracked tension panels to simulate the flaw configuration typical of service. The residual strength of 2090 specimens at a given flaw (fatigue crack) size increased with decreasing test temperature from room temperature to 76 K (liquid nitrogen), and to 4 K (liquid helium). The specimens failed by plane stress fractures with numerous delaminations at all temperatures. For x2095 specimens, the residual strength was lowest at 76 K, and the failure could be either plane stress or plane strain depending on the size and shape of the surface crack.

Three conduit sheath alloys for use in fusion energy magnets were also tested. The conduits protect superconductor cables and contain liquid helium at 4 K; they must resist degradation when aging treatments are applied during superconductor fabrication, and they must sustain high stress and fatigue loading during service. Europe, Japan, and the United States have each proposed a candidate material; our purpose was to evaluate all three materials in one laboratory.

The conduit alloys tested were low carbon 316LN (0.018C), Nb-modified 316LN (0.009C, 0.05Nb) and Ni-base alloy 908. Conventional 4-K tension and fracture toughness tests showed similar yield strengths but large variations in fracture resistance. Threshold stress intensity factors at 10^{-10} m/cycle and fatigue crack growth rates (FCGR) for the conduits were then measured using a relatively new short-crack simulation method which is especially appropriate for design purposes. Results show that aging for extended periods of time (180 h at 650-700°C) produces

$M_{23}C_6$ carbide precipitates in the 316 steels, as well as $Ni_3(Al,Ti)$ precipitates in 908. This rather severe aging is sufficient to cause undesirable intergranular failures in the low carbon 316LN; Nb-modified 316LN and alloy 908 retain relatively ductile failures, but alloy 908 offers a higher fatigue threshold at 4 K.

Large Scale Tests of Composite Support Struts

Cold-to-warm struts are used in superconducting magnet energy storage plants to support superconducting magnet rings. To assess structural reliability, we tested a prototype strut design with simulated in-service thermal and mechanical conditions. The specimens are tubular, 2 m long and 25.4 cm in outer diameter. Two types of full scale qualification tests were desired: ultimate compressive strength tests and compressive cyclic fatigue tests. This required loading the composite tube in excess of 3000 kN, with an imposed thermal gradient (4 to 295 K) over the length of the tube. To meet these specifications, we installed a cryostat in a 4.4 MN capacity servo-hydraulic mechanical test machine, creating the largest cryogenic test apparatus in the United States (Figure 16).

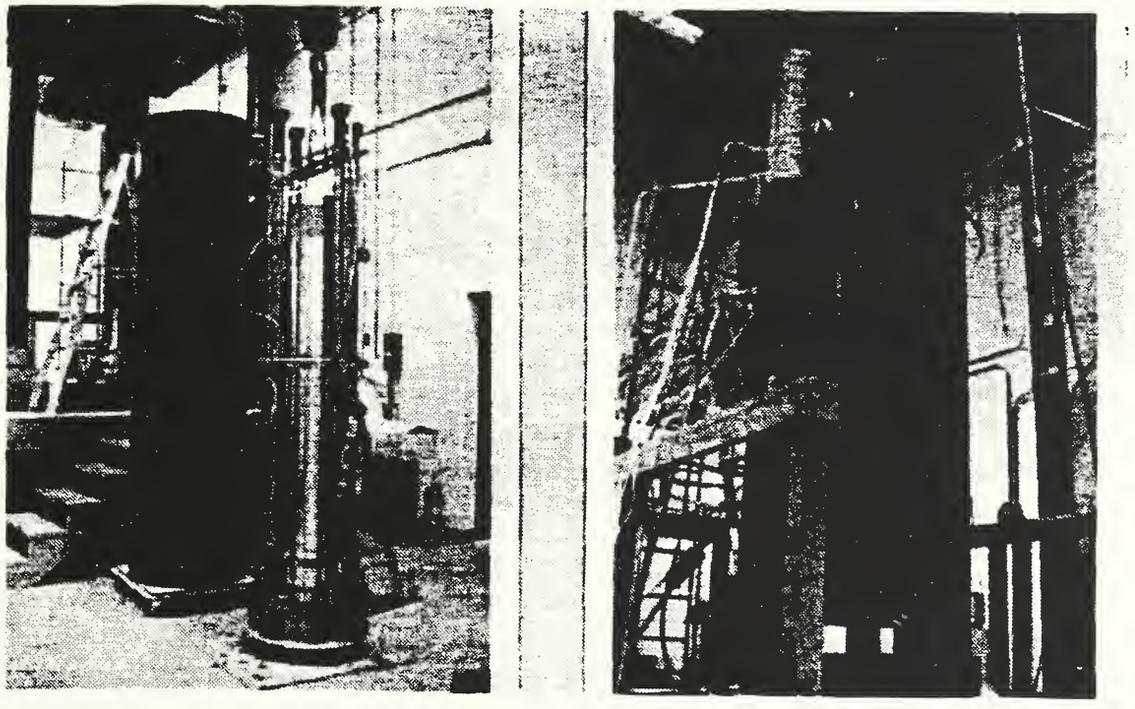

Figure 16. 4.45—MN (1000-kip) Test Machine and Cryostat.

The struts are fiber-reinforced polymer (FRP) composite tubes that must withstand cyclic compressive loads in a vacuum environment, at temperatures ranging from cryogenic (1.8 K) to ambient (295 K). The specimens were equipped with end fittings to prevent brooming at the tube ends. They were tested between two compression platens; one platen was maintained at room temperature while the other was cooled in a vacuum chamber, mainly by conduction, with liquid helium (4 K) and liquid nitrogen (76 K) flowing through tubing. Load, displacement, and temperature data were recorded with a computerized multi-channel data acquisition system.

An important conclusion is that the end fittings must be redesigned to achieve optimum results. For example, one full scale specimen (full length, 2 m) was equipped with rigid aluminum end fittings. This specimen failed in the cold region where the local temperature was 140 K, and the specimen's ultimate strength was 518 MPa (75 ksi), nearly 20% lower than expected. This specimen failed catastrophically by a combination of failure modes: shell buckling, column buckling, and longitudinal cracking. The metal end fittings exhibited circumferential cracking on their exterior surfaces, and are implicated in the failure of the tubes. Thus, end fitting design must also be taken into account to realize the full strength of the composite struts.

Compression–Shear Tests of Vacuum-Impregnated Composites

To evaluate filament-reinforced, epoxy-resin systems at cryogenic temperatures, we proposed a new compression-shear test for stainless-composite-stainless sandwiches.

Superconducting magnets for fusion energy systems require insulation that can be applied in the field to components that are subsequently heat treated and subject to simultaneous shear and compression stresses. Some designs call for fiberglass layers to be vacuum-impregnated with an epoxy resin system having a low viscosity and a long (~24-h) set-up time. Moreover, conceptual designs of fusion reactors, such as the International Thermonuclear Experimental Reactor, project a radiation dose of about 5×10^7 Gy at 4 K for the insulation systems during service. Thus, a new test is required to measure the interrelation of compression and shear stresses on composites bonded to metals, and screening tests will require specimens that are small enough to be irradiated and tested under cryogenic conditions.

The new fixture, shown in Figure 17, is used with a screw-driven test machine (10 kN maximum load). When the device is compressed, the center piece is free to move; there is no shear constraint, and indeterminate shear strain does not accumulate in the specimen before failure. Fixtures with test angles θ of 0°, 15°, 30°, 45°, 60°, 75°, or 90° are used to vary the compression–shear ratio.

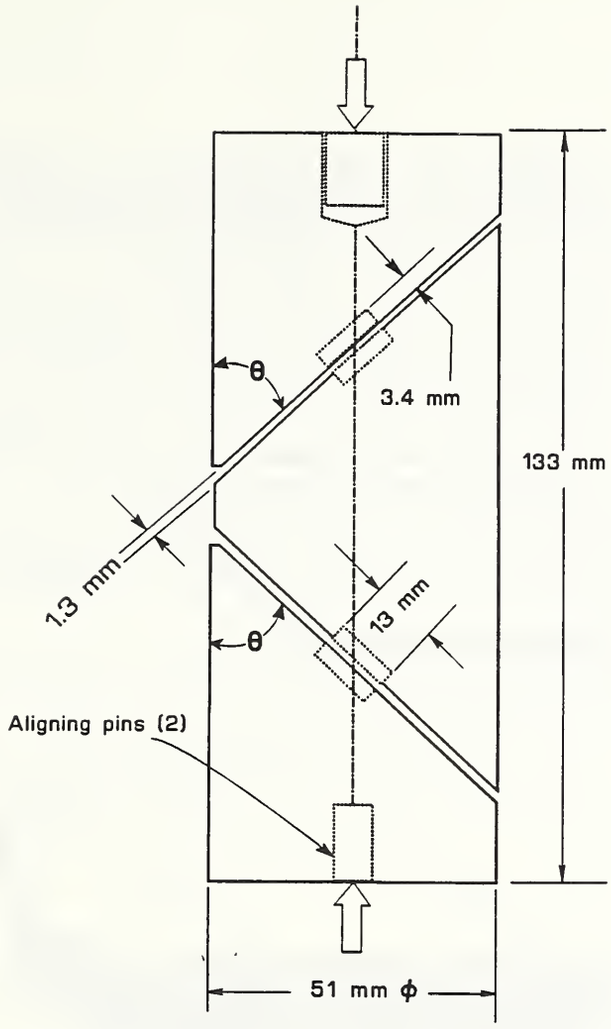

Figure 17. Compression-shear test fixture.

Sandwich-style specimens are shown in Figure 18a. To simulate magnet fabrication conditions, the specimens are vacuum-impregnated with epoxy in a mold, as indicated schematically in Figure 18b. The surface treatment of the chip can be varied, and the mold design allows for the simultaneous fabrication of 62 specimens. This permits preparation of many specimens with identical resin cure conditions so that the effect of parameters such as chip surface finish and type, as well as fiberglass surface finish, volume fraction, and layup, can be examined.

Fixture evaluation, methods of specimen preparation, and preliminary screening tests were carried out in parallel. We found that: (1) An equally-loaded shear-compression tests of fiberglass reinforced epoxy specimens, a rougher, 100-grit surface finish resulted in higher average shear strength than a finer, 250-grit finish; (2) use of a coarse, more open plain weave of E-glass improved the shear strength in failures that were primarily adhesive; (3) shear strength of the S-glass plain weave, intermediate in areal density between the two E-glass weaves tested, is comparable to the best results with high areal density E-glass; (4) "pure" shear strengths at $\theta = 0°$ are apparently 2 or 3 times lower than the shear strengths measured with an equal compressive load applied in a 45° test fixture. The results of our

initial screening tests will be used to prepare specimens for future irradiation testing at Garching, Germany.

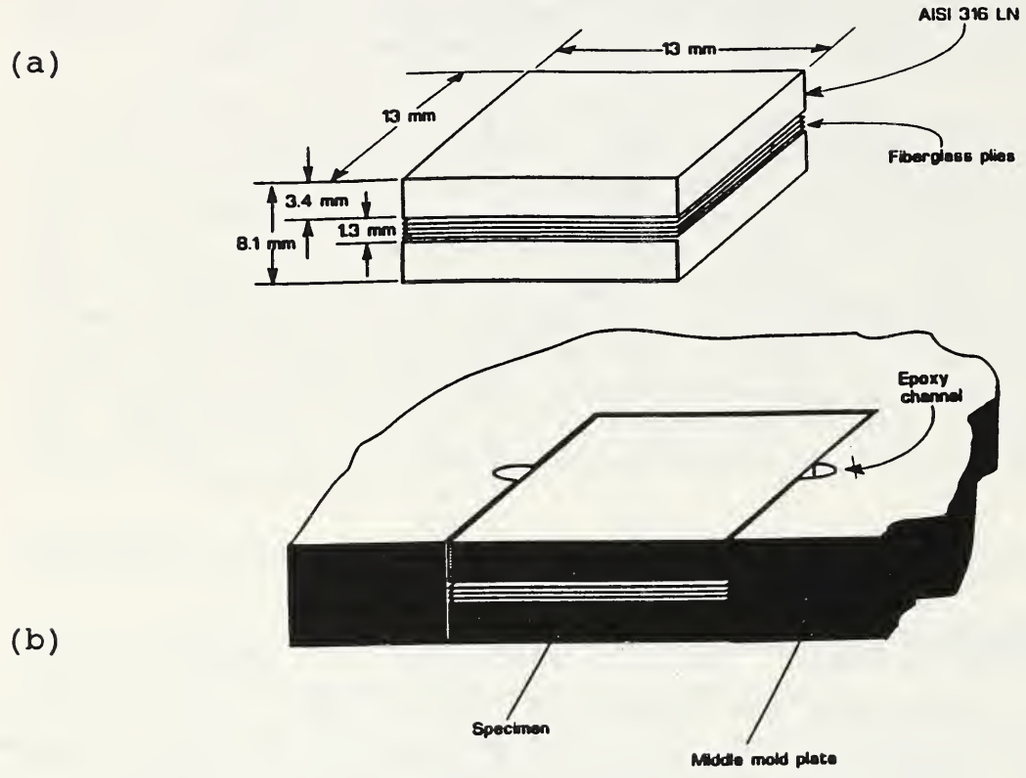

Figure 18. Composite compression-shear test specimens (a), and impregnation method (b).

Technology Transfer Highlights

Our research results are transferred to the cryogenics community through annual reports and workshops, data compilations disseminated in handbook form, and other documents such as draft test standards. Highlights for 1991 are summarized below.

A U.S.–Japan workshop on Low Temperature Structural Materials and Standards was organized and held on June 10, 1991, in Huntsville, Alabama.

"Aluminum Alloys for ALS Cryogenic Tanks: Comparative Measurements of Cryogenic Mechanical Properties of Al-Li Alloys and Alloy 2219," NISTIR (March, 1991) was prepared and published.

A critical review of irradiation effects on fiberglass–epoxy composites was initiated to guide future research in this difficult area. Weaknesses in the available database are identified: (1) E-glass reinforcement, rather than the more radiation resistant S-, R-, or T-glass has often been used; (2) radiation spectra have been used that do not simulate the expected fusion spectrum at toroidal field magnets; (3) the cryogenic test temperatures often were not low enough, and warm-up and recovery often occurred before testing after irradiation. The "Standard Test Method of Tension Tests for Structural Alloys in Liquid Helium" was approved by the American Society for Testing and Materials, Main Committee E 28. NIST personnel wrote the standard, made the necessary revisions, and responded to the comments by national and international reviewers.

A revision of "Standard Test Methods for Notched Bar Impact Testing of Metallic Materials", ASTM Method Designation E 23-91, was also approved by Main Committee E 28. This greatly affects the practice of Charpy testing at temperatures below 77 K. NIST proposed the revision based on results of cooperative studies with other laboratories in the U.S. and Japan.

Physical Properties

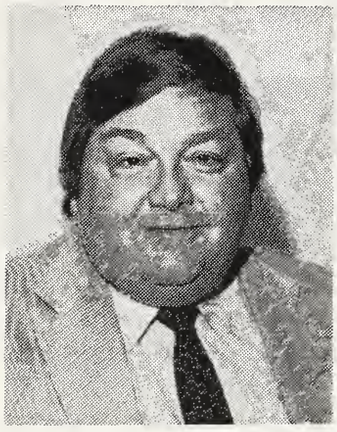

Hassel Ledbetter
Research Leader

T. Ashizawa,* D. Balzar,** M. Földeáki†, S.A. Kim, M. Lei,∫, S.-H. Lin§

Our research emphasizes measurements and modeling of elastic constants and related physical properties of metals, alloys, composites, ceramics, and the new high-T_c oxide superconductors. For many studies, the temperatures range between 295 and 4 K. The elastic constants, which relate deformation to stress, sustain our interest because they relate to fundamental solid-state phenomena: interatomic potentials, equations of state, and phonon spectra. Furthermore, thermodynamics links elastic constants with specific heat, thermal expansivity, atomic volume, and the Debye temperature.

In recent years, our research efforts have fallen into four categories:

1. austenitic steels,
2. composite materials,
3. high-T_c oxide superconductors
4. other materials.

---

* Visiting scientist from Hitachi Chemical Company, Japan.
** Visiting scientist from Physics Department, Faculty of Metallurgy, University of Zagreb, Yugoslavia.
† Visiting scientist from Institute for Materials Testing and Quality Control, Budapest.
∫ Graduate student from Institute of Metal Research, Shenyang, China. Now at Los Alamos National Laboratory
§ Graduate student from Physics Department, Tsinghua University, Beijing, China. Now at Physics Department, University of Colorado, Boulder.

Representative achievements and accomplishments

- Between 5 and 400 K, we studied the magnetic susceptibility of three f.c.c. Cr–Mn austenitic steels, both annealed and deformed. Comparison between measurements and a generalized molecular-field theory revealed type-1 antiferromagnetism. Both atomic moment and molecular-field coefficients depend strongly on metallurgical history.

- We determined the complete elastic constants for seven Al_2O_3/Al spherical-particle-reinforced composites. Measurements and model agree well. The model consisted of the long-wavelength limit of a scattered-plane-wave ensemble-average quasicrystalline sum over pairs.

- In $(La–M)_2CuO_4$ superconductors, we discovered a surprising $T_c–\Theta_D$ relationship. Thus, the critical temperature depends on the average phonon properties, as in the BCS model. But T_c increases with increasing Θ_D, contrary to McMillan's model where the electron–phonon parameter λ varies as Θ_D^{-2}.

- We derived a simple relationship between the volume change $\Delta V/V$ and the elastic constants, second-order and third-order, which does not require the elastic-constant temperature dependence.

Below, we give a complete list of research completed during the last year. The twenty-six titles represent published studies, manuscripts submitted for publication, or abstracts offered for presentation at forthcoming technical meetings.

<u>Austenitic steels</u>

1. Magnetic-susceptibility–temperature peaks in Fe–Cr–Ni alloys.

2. Magnetic properties of Cr–Mn austenitic stainless steels.

For the latter study, the magnetic susceptibility χ of three Cr–Mn austenitic stainless steels was measured versus temperature in the range 5–400 K. All specimens showed a characteristic susceptibility maximum. The temperature of the maximum and especially the curve shape depend strongly on specimen composition and metallurgical condition (as-quenched, deformed). Because no significant field dependence appeared, the susceptibility maximum was identified as the antiferromagnetic Néel temperature. $\chi(T)$ measurements above T_N were fitted to a modified Curie–Weiss equation. Comparison between measurements and generalized-molecular-field-theory predictions allowed us to identify the magnetic structure as that of a first-type antiferromagnet with f.c.c. crystal structure. The atomic magnetic moment and the molecular-field coefficients depend strongly not only on composition, but also on metallurgical prehistory, that is, on the degree of the applied mechanical deformation and heat treatment.

Mainly, manganese affected the antiferromagnetic interactions, while chromium affected the ferromagnetic. Mn and Fe contributed the most to the effective atomic moment. Measurements on mechanically deformed specimens show a structure sensitivity of the molecular-field constants. This could be interpreted consistently in terms of lattice-parameter changes. The apparent structure sensitivity of the effective atomic moment can be attributed to changes in matrix composition caused by precipitation. Figure 19 shows a typical result for $\chi(T)$.

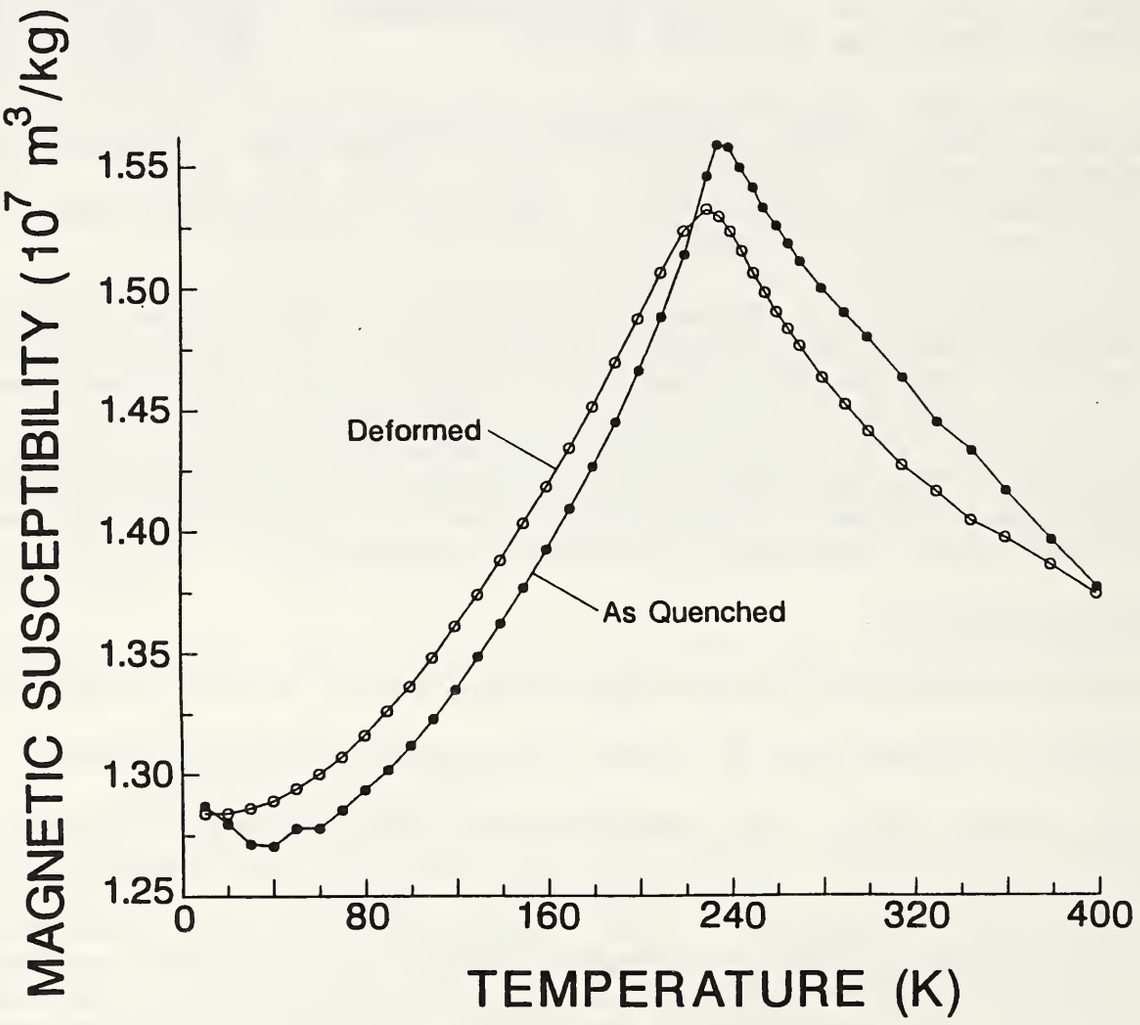

Figure 19. DC magnetic susceptibility χ versus temperature for an f.c.c. Fe–18Cr–19Mn alloy. $\chi(T)$ peak corresponds to a paramagnetic–antiferromagnetic (type 1) transition during cooling. Mechanical deformation blunts the $\chi(T)$ cusp and moves it to lower temperatures.

Composite materials

1. Elastic constants of a tungsten-particle copper-matrix composite.

2. Elastic constants of fiber-reinforced composites: a fresh measurement approach.

3. Thermal expansion of an SiC-particle-reinforced aluminum composite.

4. Elastic properties of uniaxial-fiber reinforced composites: general features.

5. Dynamic Young modulus of a ceramic-aluminum particle-reinforced composite: measurement and modeling.

6. Elastic properties of Al_2O_3/Al composites: measurement and modeling.

In the last study, we considered seven Al_2O_3-particle-reinforced Al-matrix composites with particle volume fractions ranging from 0 to 0.24. At ambient temperature, we measured the elastic constants by two dynamic methods: kilahertz resonance and megahertz pulse-echo-superposition. We report the usual elastic-constant set: bulk, shear, Young moduli, and Poisson ratio. The microstructures show a random distribution of spherical particles, from specimen to specimen ranging from 30 to 100 μm. The highest observed Young-modulus anisotropy was 1.04. To model this system, we used the long-wavelength limit of a plane-wave ensemble-average method. The model estimates the speed of a plane harmonic wave, averages the scattered field by the Waterman—Truell procedure, and uses Lax's quasicrystalline approximation to sum over pairs. Measurements and modeling agree well: the average disagreement in the Young modulus is about one percent. As expected, except for the Poisson ratio, all measurements fall below a linear rule-of-mixture. Figure 20 shows modeling and measurement results for the Young modulus.

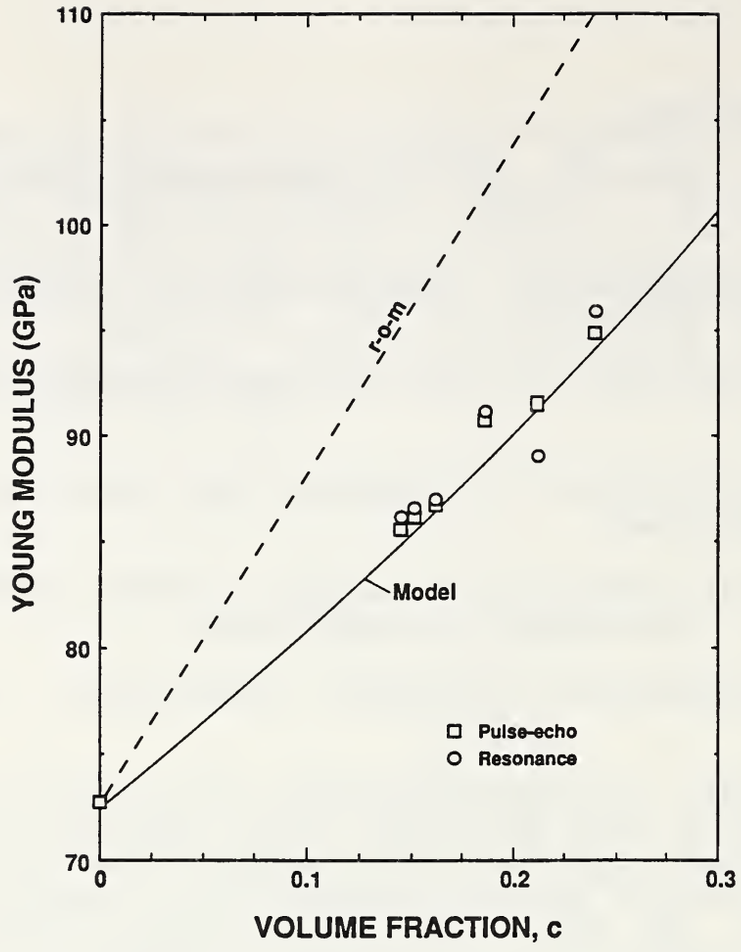

Figure 20. Young modulus versus temperature for a series of Al_2O_3/Al spherical-particle-reinforced composites. Circles and squares represent kilohertz and megahertz measurements. The dashed line represents a linear rule-of-mixture. The solid line represents our model calculation. The model represents the long-wavelength limit of a scattered-plane-wave ensemble-average quasicrystalline average over pairs.

Oxide superconductors

1. Oxides and oxide superconductors: elastic and related properties.

2. Group and phase sound velocities in an $Eu_1Ba_2Cu_3O_7$ superconductor and related perovskite oxides.

3. Monocrystal elastic constants of orthotropic $Y_1Ba_2Cu_3O_7$: an estimate.

4. Estimated dT_c/dP and $dT_c/d\sigma_{ij}$ for the $Y_1Ba_2Cu_3O_7$ superconductor.

5. Elastic constants of polycrystalline $Y_1Ba_2Cu_3O_x$.

6. Correlation between T_c and elastic constants of $(La-M)_2CuO_4$.

7. Stacking faults and microstrain in $(La-M)_2CuO_4$, M = Ca, Ba, Sr.

8. Elastic properties of $Bi_2Sr_2Ca_1Cu_2O_8$ and $Ba_2Sr_{1.5}Ca_{1.5}Cu_2O_8$.

9. Stacking faults and microstrain in $La_{1.85}M_{0.15}CuO_4$ (M = Ca, Ba, Sr) by analyzing x-ray diffraction line broadening.

10. Magnetic studies of $Pr_{2-x}Ce_xCuO_{4-\delta}$.

11. Elastic constants and Debye temperature of $Y_1Ba_2Cu_3O_x$: Effect of oxygen content.

12. Magnetic susceptibility of Pr_2CuO_4 monocrystals and polycrystals: field and temperature dependences.

13. Critical-temperature/Debye-temperature correlation in $(La-M)_2CuO_4$ superconductors.

In the last study, we considered three $La_{1.85}M_{0.15}CiP_4$ compounds with M = Ca, Ba, Sr. By measuring ultrasonic sound velocities, we determined the acoustic Debye temperature Θ_D, which at T = 0 K equals the specific-heat Debye temperature. Like conventional BCS materials, T_c depends regularly on Θ_D. Unlike BCS materials where T_c decreases with increasing Θ_D (lattice softening increases T_c), in La–M–Cu–O, T_c increases with increasing Θ_D. The reason for this difference lies in how the electron–phonon parameter λ depends on Θ_D. In McMillan's analysis, $\lambda \sim \Theta_D^{-2}$. Thus, for conventional materials, the T_c–Θ_D curve increases, passes through a maximum at $\lambda = 2$, and then decreases. The present results for La–M–Cu–O show that T_c increases continuously with Θ_D. Keeping the usual $T_c(\Theta_D, \lambda)$ models requires us to abandon the usual $\lambda \sim \Theta_D^{-2}$ relationship and adopt $\lambda \sim \Theta_D^n$, where $n > -\lambda$. This new λ–Θ_D relationship allows T_c to increase continuously with increasing Θ_D. Figure 21 shows the T_c–Θ_D variation together with the a–Θ_D variation, where a denotes a unit-cell parameter.

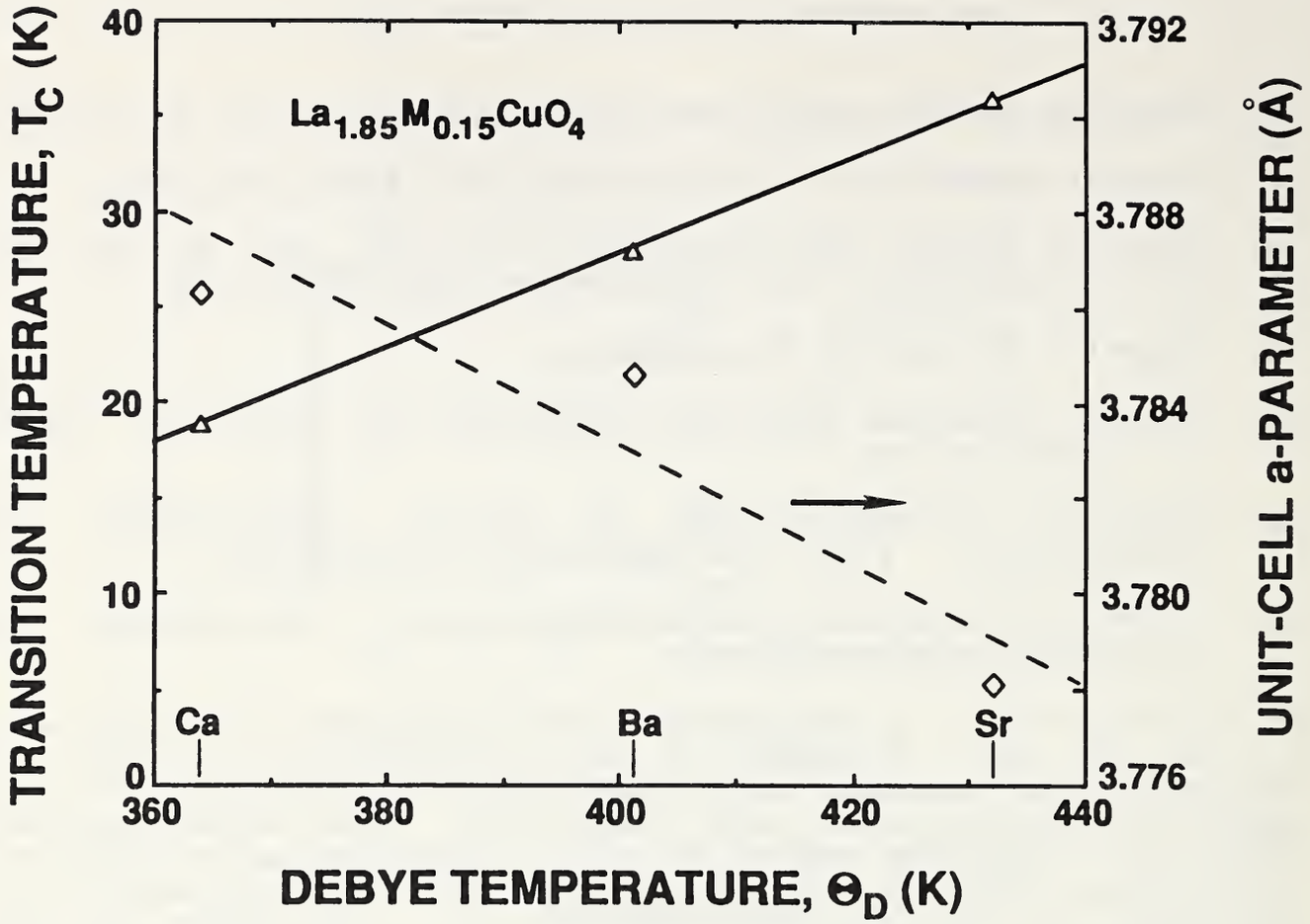

Figure 21. Dependence of critical temperature T_c and unit-cell a-parameter on Debye characteristic temperature Θ_D. Note that both properties behave contrary to intuition, departing from the periodic-table Ca, Sr, Ba sequence.

Other materials

1. Atomic frequency and elastic constants.

2. Elastic and electric constants of piezoelectric solids by resonant ultrasound.

3. Elastic constants of an orthotropic-symmetry particle-reinforced metal-matrix composite by a solid-resonance method.

4. Profile fitting of x-ray diffraction lines with a Fourier-method analysis.

5. Thermal expansion and elastic constants.

In the last study, we derived a simple, useful relationship between thermal expansion $\Delta V/V$ and elastic constants. The relationship permits estimation of thermal expansion from only elastic constants (second-order and third-order) and atomic volume. Elastic-constant temperature dependence is not required. We tested the relationship for a variety of crystalline solids. Considering 0–293 K region,

measurement-calculation disagreement ranges from less than 1 to 15%. The model permits extrapolation of high-temperature (near-linear) thermal expansion to zero temperature. Figure 22 shows the study's principal result.

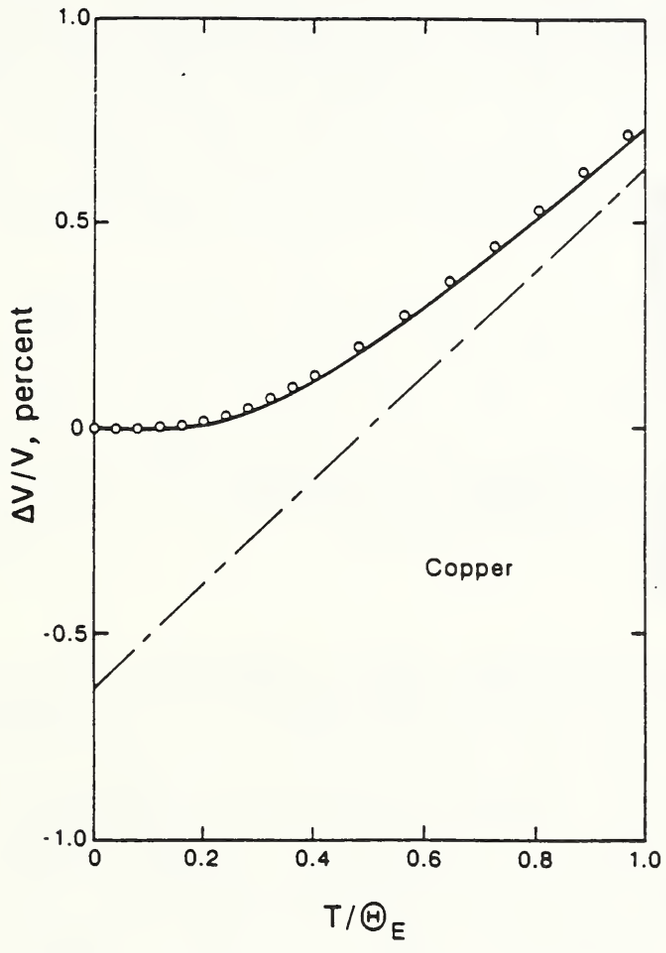

Figure 22. For copper, the volume changes between T = 0 and T = Θ_E, the Einstein temperature. Open circles represent observed values. The solid line represents our model calculation. The dashed line represents linear extrapolation from high temperatures. Its intercept at T = 0 gives the zero-point energy contribution to volume. Lowering the Θ_E from 248 to 243 K gives exact (to the eye) agreement between theory and measurement.

MATERIALS PROCESSING

The Welding and Thermomechanical Processing Groups measure and model the physical and metallurgical changes that occur during material processing, such as metal transfer in arc welding, recrystallization, and phase transformation. These changes affect the quality, microstructures, properties, and performance of metals.

Welding

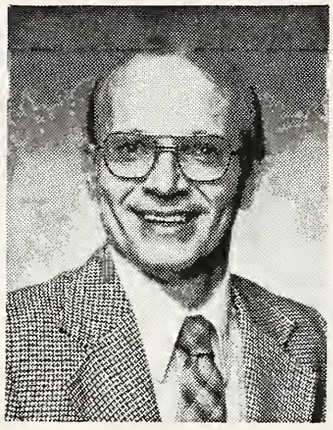

Thomas A. Siewert
Group Leader

M. W. Austin, B.R. Danley*, R. B. Madigan, C. N. McCowan, M. A. Mornis**, T. P. Quinn, D. A. Shepherd, D. P. Vigliotti

The Welding Group conducts materials research to improve the quality, reliability, and safety of welded materials. Our goals include the development of sensors, measurement procedures, and controls that can automate the production of consistent, high quality welds. A specific goal for a Navy-sponsored program is to develop a more fundamental understanding of the process of droplet transfer across the arc, then incorporate this information into an intelligent weld controller that improves the quality and efficiency of welding.

The Welding Group is also responsible for radiology NDE and the Office of Standard Reference Material (OSRM) Charpy V-notch calibration program.

---

* Research Associate from the AC-Rochester Division of General Motors, Milwaukee, Wisconsin

** Graduate Student, Colorado School of Mines, Golden, Colorado.

Representative accomplishments

- An arc sensor module has been developed and is being delivered to Babcock and Wilcox as part of a Navy-sponsored program. It contains algorithms that simulate the ability of a welder to detect various sources of weld defects. It is being integrated with other sensors into an autonomous welding system.

- In cooperation with Image Quality Incorporated, we produced a series of aluminum welds and their radiographs in a program for the U.S. Army. The welds contained a variety of flaw types and degrees that spanned the range of flaws commonly observed in aluminum welds. This series of radiographs has been reviewed by several ASTM Committees, and has been proposed as a series of standard reference radiographs for aluminum welds.

- Several new image quality indicators and measurement devices were developed for radioscopy systems. These include a calibration board for measuring the repeatability of the specimen stage's x- and y-axis drives, a device for measuring focal spot size of microfocus x-ray tubes, and a device for measuring the z-axis resolution of a laminography system. These new indicators and devices are now being evaluated in a series of round robins.

Arc Sensors

Our welding laboratory activities continue to generate cooperative programs with industry and other government agencies. A major program with the U.S. Navy is to develop our though-the-arc sensing concepts into an industrial-grade sensor module for gas metal arc welding. We have completed the first version of this module which consists of software (which incorporates the knowledge used by a welder to correct for welding problems), a host personal computer, and input/output devices. It is designed to interface with a host computer, which would decide whether problems detected by the system can be corrected while welding, or whether the welding should be terminated until the problems has been corrected.

The module monitors the weld current and voltage. After the measurements are processed (by standard deviation and power spectrum calculations), the process data are compared to reference data. The present version of the module can detect trends in the voltage and current values, detect undesired short circuit events in the spray transfer mode, and determine contamination or loss of the gas shield. It is being modified to detect droplet detachment and estimate remaining contact tube life. The module will be evaluated at Babcock and Wilcox, the prime contractor to the Navy.

A second interaction is with the AC-Rochester Division of General Motors. They have assigned a research associate (B. Danley) who will spend about four months working on our projects, while

evaluating how this technology can be applied to their welding systems.

To meet the expanding needs of our research programs, our laboratory capabilities have been upgraded substantially. We have added a pulse welding power source, of the type to be used in the Navy program. The power source has been modified with a special voltage (noise) filter that can be switched in and out of the circuit. We are evaluating how the output characteristics of this power source (with and without the filter) affect the natural response of the arc and compare to previous data obtained with a very stable power source.

We have also improved the optical train of our laser vision system. This vision system back-lights the arc, while filtering the high intensity light generated by the arc. It permits comparison of the sensor output with the arc characteristics, for calibration. The arc characteristics are recorded with our high speed video system (1000 Hz in the full frame mode and 6000 Hz in the partial frame mode).

The present data acquisition system consists of a 25-MHz processor, integral math co-processor, and high-speed cache. The analog-to-digital board was replaced with a 100 kHz bipolar version, for better resolution of differential signals.

Weld Process Modelling

Theoretical modelling efforts have been undertaken to facilitate automatic control of the gas metal arc welding (GMAW) process. The electrode extension determines the amount of power used in GMAW and, therefore, is an important variable to control to ensure repeatable, high-quality welds. The electrode extension was predicted using a one-dimensional model of the melting electrode. Joule heating in the electrode, heat directly applied to the end of the electrode from the condensing electrons, and heat transferred from the droplet, together with conduction along the electrode were considered. The thermal conductivity, the thermal diffusivity, and the electrical resistivity of the material were allowed to vary with temperature. The resulting one-phase Stefan problem was solved numerically using a nonlinear transformation to fix the melting boundary. The steady state electrode extension was predicted to an accuracy of 1.9 mm. The onset of short circuiting as the current is decreased was predicted within 9%. The method of describing functions showed that the magnitude of the response of the electrode extension to sinusoidal perturbations in the current with a given amplitude monotonically decreased with increasing frequency. Higher mean current also decreased the magnitude of the response in electrode extension. The response in the electrode extension was linear in the amplitude of the excitation in the current up to 32% of the mean.

Work has been initiated to better understand the transfer mechanism of droplets from the melting electrode to the weld pool. The frequency at which the droplets are detached as well as droplet size and droplet velocity help to determine the final weld geometry and quality. Par Jonnson, a graduate student working under NIST sponsorship for Professor Julian Szekely at the Massachusetts Institute of Technology, is modelling droplet detachment using a fluid dynamics model of the arc and the melt at the electrode end. A steady state model of the plasma arc in GMAW will be combined with a free boundary model of the drop. The free boundary model will include electromagnetic forces, surface tension, surface tractions from the arc, circulation within the drop, and the heat transferred to the drop from the arc. Approximate governing equations have been identified and work on a finite difference solution technique is proceeding.

X-Ray Radioscopy Standards

X-ray radioscopy refers to x-ray inspection systems in which the conventional film imaging media has been replaced with an imaging screen, and which also often have low-light-level cameras and video display monitors. Systems with this electronic viewing capability can be automated further with automatic inspection routines and motorized stages. Unfortunately, the standards and techniques necessary to confirm the proper operation of these systems are not yet available. This program supports efforts to develop the necessary standards and techniques so these efficient inspection technologies can replace older techniques with no loss of control.

We have been working closely with American Society for Testing and Materials (ASTM) Subcommittee E07.01 on Nondestructive Testing. This committee includes representatives of the industrial developers and users of this technology, and is responsible for maintaining a wide variety of x-ray testing procedures and standards. We have been assisting in the preparation of new standards for radioscopy, that parallel the older standards for film-based radiography.

The rest of the x-ray inspection community is also quite interested in implementing this new x-ray inspection technology. International Institute of Welding Commission V is developing a number of standards for this technique, which they will submit to the International Standards Organization as draft standards. We are trying to serve as liaison between ASTM and IIW so U.S. standards will be compatible with the rest of the world.

At the January 1991 ASTM meeting and July IIW meeting, we presented a twisted strip image quality indicator design for characterizing a microfocus x-ray tube beam. The concept is simply that of a thin strip with a half twist. The twist allows the long dimension of the strip cross section to be perfectly oriented with the x-ray beam at some location, without careful orientation of the strip

itself. We have found metal strip is readily available in thicknesses that provide a high-contrast image. Figure 23 shows the intensity gradient across an image of the strip. The 0.07-mm width demonstrates the good resolution possible with the technique. The concept is being evaluated in round robins within ASTM and IIW for measurement of image unsharpness and focal spot size. We plan to summarize the results at the next ASTM and IIW meetings.

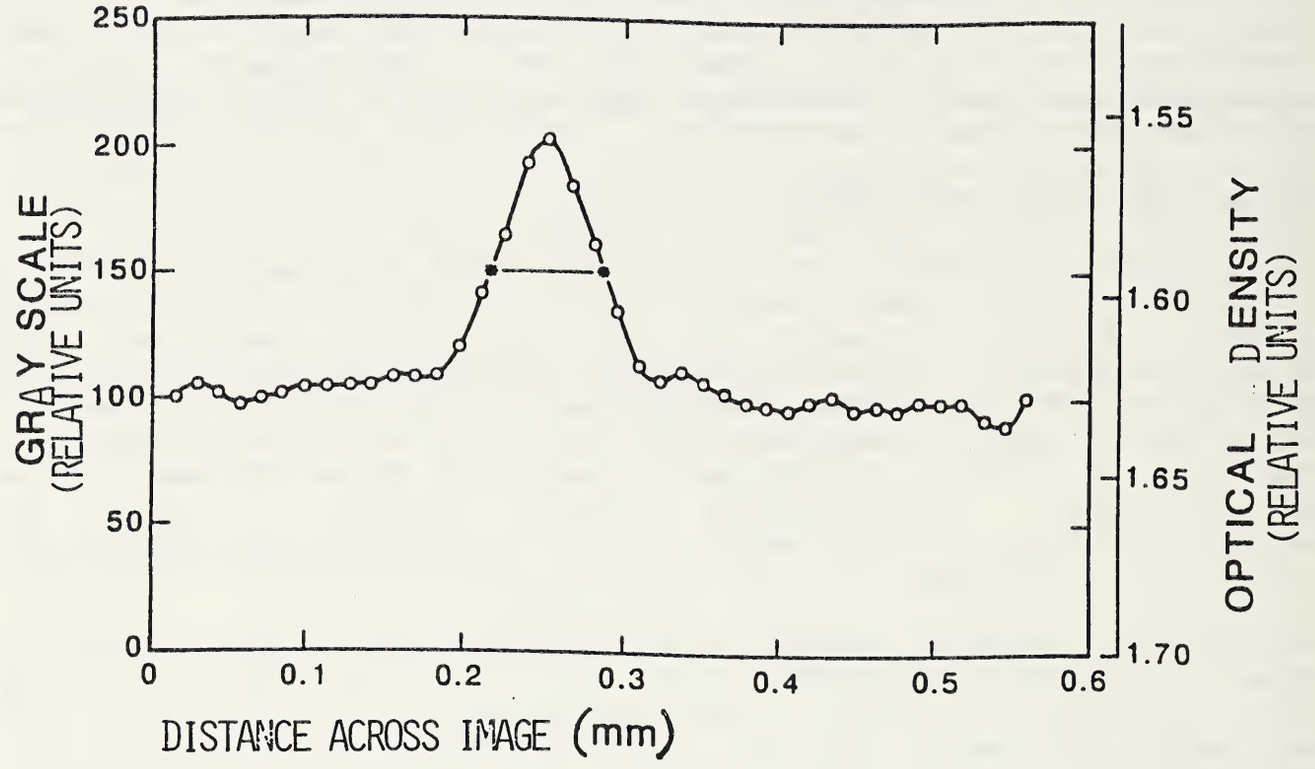

Figure 23. Gray-scale intensity across the image of the twisted strip image quality indicator.

Fiber-volume fraction and porosity of polymer composites is of concern to those using these materials for high-performance structures. Since the constituents of a composite (fiber, matrix, and porosity) have differing x-ray attenuation coefficient and the energy dependence of the coefficients vary, it is possible to formulate an inversion algorithm for recovering the percentage of each constituent from attenuation measurements at three or more energies. An apparatus for making quantitative x-ray transmission measurements on composites has been assembled. The system (Figure 24) utilizes an energy-sensitive NaI(Tl) detector and a PC-based multichannel analyzer. Transmission spectra were collected for various samples of glass-epoxy composites and demonstrate the

utility of the concept. The measurement method appears promising in cases where the x-ray attenuation characteristics of the fiber and matrix separately are known a priori or can be measured. The system stage will be automated next year for spatial mapping of the composite properties.

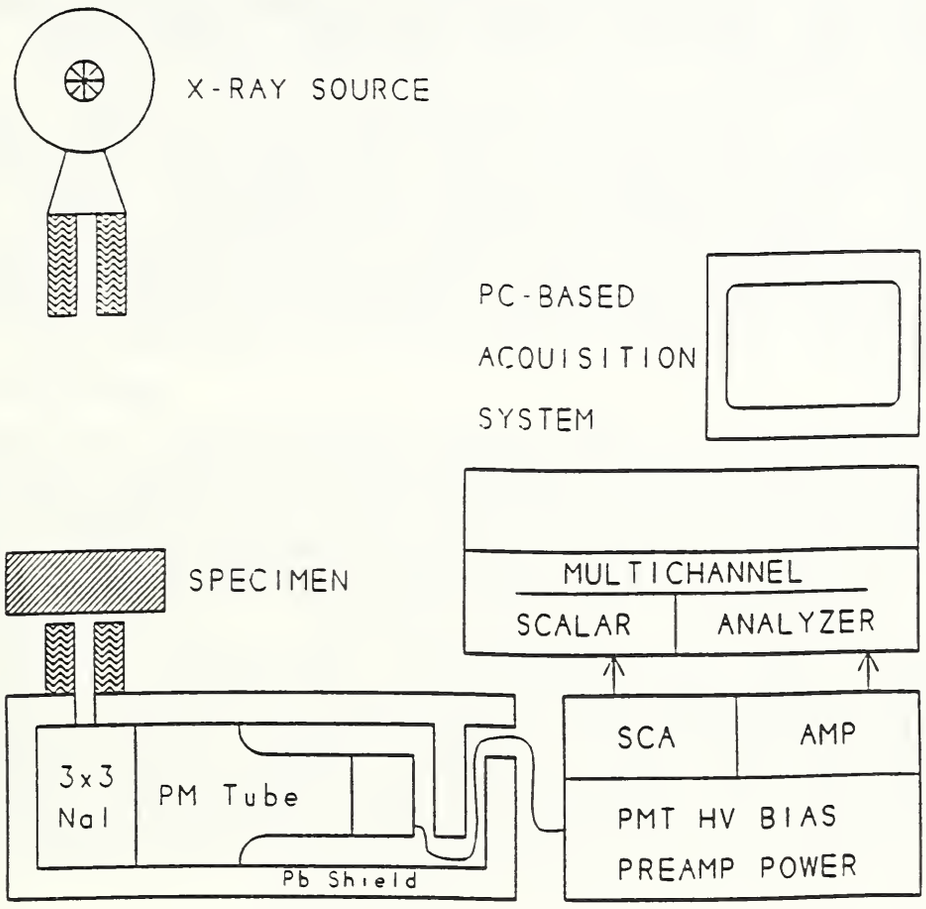

Figure 24. Schematic of our prototype system for in-situ measurement of fiber-volume in composite materials.

NIST has been working with the General Electric Company, the Naval Air Engineering Center, and the U.S. Army Materials Technology Laboratory in developing a military standard for radioscopic inspection. The standard will be a supplement to a general ASTM standard (E1255) on radioscopic inspection. The fifth draft of this standard has been circulated for comments and we are nearly ready to coordinate it through Department of Defense Laboratories.

Evaluation of an X-Ray Laminography System

X-ray laminography, a tomographic technique that can examine individual planes of focus within a three-dimensional structure,

promises to be an excellent method of inspecting complicated circuit boards. However, this new technology has not been in existence long enough to possess the variety of accuracy and precision measurements necessary to prove its suitability as a quality control scheme. In fact, we were unable even to locate image quality indicators that could be used to generate these measurements for laminography systems. Therefore, our program to evaluate the technical merits of a laminography system included the development of special image quality indicators and other calibration devices.

We purchased a commercially available laminography system (with U.S. Army funds) to measure its suitability for circuit board inspection. To evaluate system reliability in an industrial environment, we performed a series of thermal and electrical stress tests, while monitoring the system performance by the X and Y dimension resolution and the contrast transfer function. The system was also evaluated externally in circuit board inspection applications.

To develop measures of the system performance, we constructed a series of 300-mm-square boards (similar in size to the circuit boards normally inspected with the system) and populated them with devices that could measure the system performance. Some boards included a series of holes that were used to measure the X and Y dimension resolution of the system. Independent optical measurement of the hole positions formed the reference for the measurement. We also developed a new type of image quality indicator for measuring the Z dimension resolution. Another board contained an x-ray line pair gage. Images of this gage were sent to an image processor where we produced a plot of image contrast versus line spacing. This plot, the contrast transfer function, provided a more precise characterization of the system performance than a single value of spatial resolution.

The prototype X and Y dimension calibration board is being evaluated in a round robin, which includes a variety of laminography systems. These users include electronic board producers (with both government and industrial contracts), as well as the manufacturer of the laminography system. Upon successful completion of the round robin test, a series of these boards will be constructed, calibrated, and distributed through the Office of Standard Reference Materials to users of laminography systems (or other automated x-ray systems) as a standard device for system calibration.

Charpy V-notch Calibration Program

The Charpy impact test is a small-scale laboratory and industrial fracture experiment that uses a pendulum-type drop hammer and a centimeter-size material specimen to measure the ductile or brittle behavior of steel. It is the most widely used standard for

predicting the fracture behavior of steel because of its simplicity and low cost. We evaluate the results from the fracture of standardized specimens, results that are used to certify the accurate operation of these machines. We have preformed these evaluation services for about 1000 machines, from around the world, during the past year.

Two specimen energy ranges (near 17 and 98 J) continue to be available, and a super high energy range (near 160 J) was added this year. During the next year, we plan to add an intermediate energy range (near 55 J) to align the certification procedure with changes being balloted within the ASTM Committee (E28) responsible for the standard. We are also evaluating new materials, for more consistent values within the existing energy ranges. An emerging problem is the growth in the use of an International Standards Organization specification which uses a different striker design. We are studying ways to bring the two standards into agreement.

Analysis of Fluxes

In support of standards development and control procedures within the U.S. Navy, we continue to evaluate techniques for the analysis of welding fluxes. Our goal is to identify a method whereby we can control the flux composition and predict welding problems such as poor bead shape or hydrogen cracking.

For many welding processes, the flux is an integral part of the electrode, and it is evaluated during qualification testing. Submerged arc welding is an exception; the electrode and flux can be combined in an arbitrary manner. Thus, qualification of one electrode-flux combination can not necessarily be transferred to another. This program is investigating the use of new evaluation techniques.

THERMOMECHANICAL PROCESSING

Research in thermomechanical processing (TMP) uses a deformation-processing simulator built at NIST. We study the metallurgical changes that occur in steels during forging and subsequent cooling. By controlling the deformation-temperature schedules, the cooling after forging, and the subsequent tempering treatment, we are striving to achieve optimum strength and toughness in directly cooled and directly quenched forging steels.

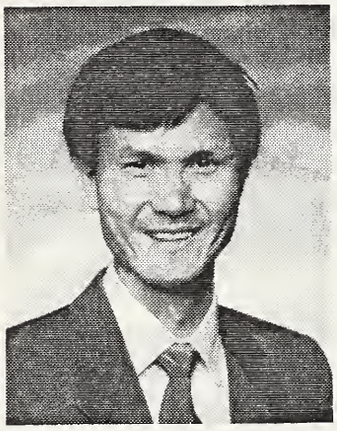

Yi-Wen Cheng
Research Leader

P.T. Purtscher, R.M. Kuziak*, A. Tomer**

Representative Accomplishments

- Experiments using microalloyed steels have been conducted to verify models predicting the austenite grain evolution during hot working.

- Flow stress of a microalloyed steel have been measured at high temperature and high strain rate. A physically based equation has been developed to mathematically describe the flow behavior.

---

* Guest researcher from the Institute of Ferrous Metallurgy, Gliwice, Poland.

** Guest researcher from the Nuclear Research Center, Negev, Israel.

Austenite Grain Evolution During Thermomechanical Processing

In steels, a fine austenite grain size is a prerequisite for obtaining fine ferrite grains that simultaneously increase strength and improve toughness. At high temperatures, austenite grains recrystallize after deformation (static recrystallization). The recrystallized grain size (d_{rex}) is a function of the grain size before deformation (d_o) and the amount of applied strain (ϵ). Sellars proposed the equation, $d_{rex} = C\ d_o^m\ \epsilon^n$, to describe the relationship for Nb-treated microalloyed steels, where C, m, and n are constants. The equation can be used for optimizing the deformation schedule to achieve the finest austenite grain sizes possible during TMP.

Our experimental results obtained to date indicate that Sellars' model works very well in cases where d_o is relatively large (57 and 137 μm). When d_o is in the order of 20 μm, the model underestimated the d_{rex}. The comparison of experimental and calculated recrystallized grain sizes are presented in Figure 25. In the figure, the x-axis is the amount of strain applied to a specimen in one deformation. The y-axis is the recrystallized grain diameter after deformation. The results show that grain refinement is most effective when d_o is relatively large.

However, little or no grain refinement can be achieved when d_o is in the order of 20 μm. Figure 25 also shows that deformation temperature, which was not taken into consideration in Sellars' model, does not affect the results significantly. For Ti-V-treated microalloyed steels, the grain size predictions by the model proposed by Roberts, et al. did not agree well with limited experimental results obtained to date. Additional experiments will be performed to check the models.

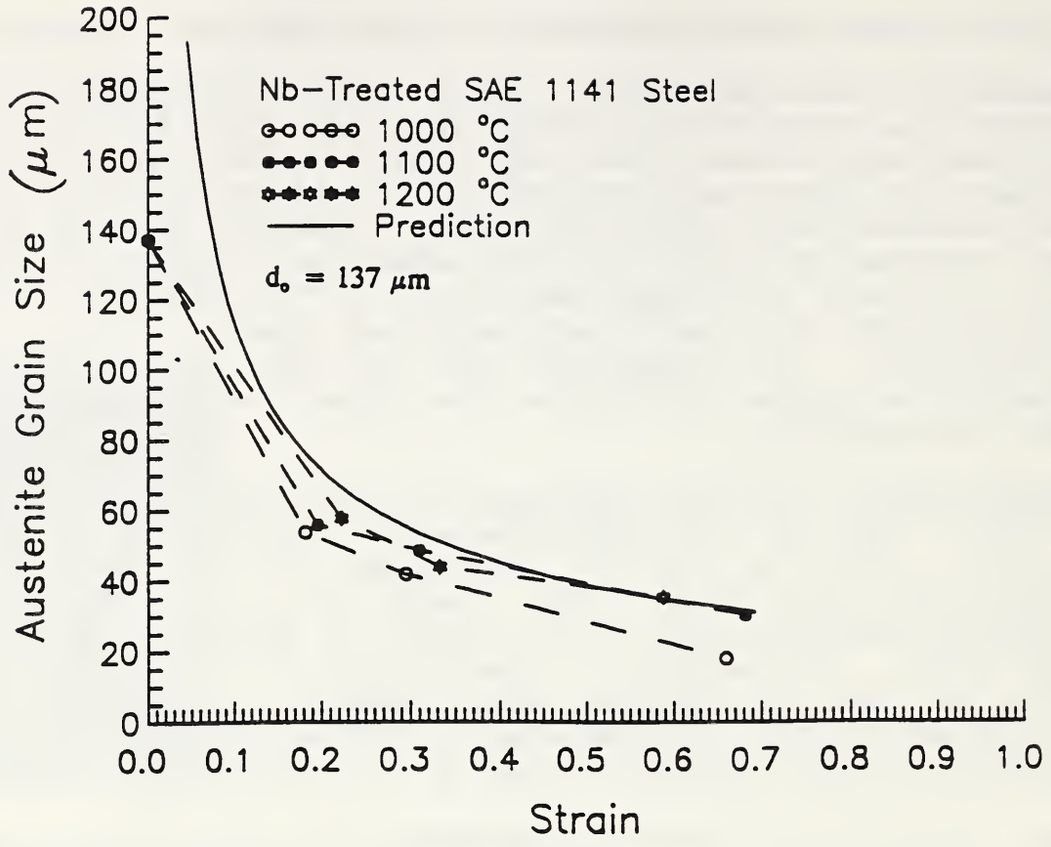

Figure 25. Comparison of experimental and calculated recrystallized grain sizes as a function strain or a Nb-treated microalloyed steel.

Stress-Strain Curves at High Temperature and High Strain Rate

For a Nb-treated microalloyed steel, stress-strain curves have been determined under different temperatures and different strain rates. Cylindrical specimens were compressed at temperatures of 900, 1000, 1100, and 1200 °C and at constant strain rates of 0.1,1, and $10s^{-1}$. The results show that the flow stress decreases with increasing test temperature. The flow stress also decreases with decreasing strain rate, except in the case when precipitation occurred at 900 °C with the strain rate of 0.1 s^{-1}. In the latter case, the flow stress is higher than that of testing at the strain rate of 1 s^{-1}. The stress-strain data have been fitted into the physically based equation $\sigma = A\ [1 - \exp(-B\epsilon)]^n$. In the equation, A is the saturation stress, B is related to characteristics of strain hardening and dynamic recovery, and n is the functional relationship between stress and dislocation density. A representative result is given in Figure 26.

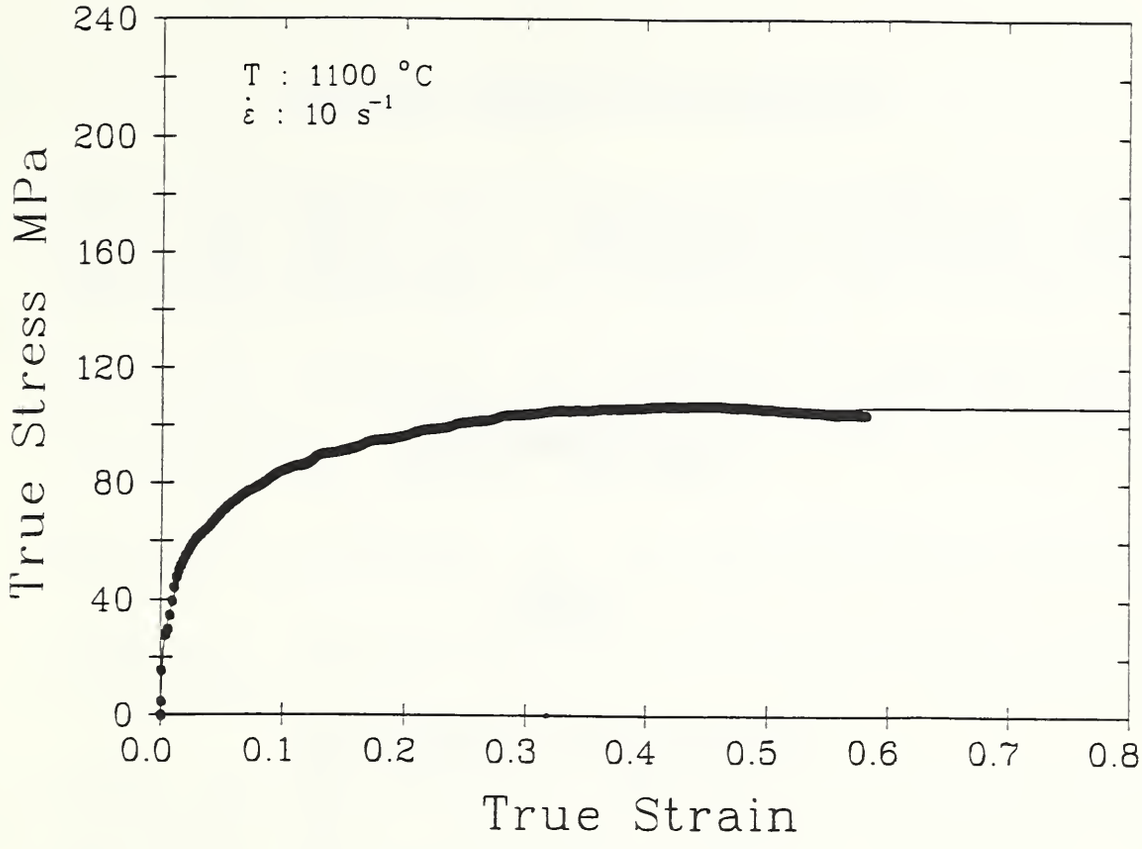

Figure 26. The stress-strain data of a Nb-treated SAE 1141 steel. The solid dots are experimental data obtained at a temperature of 1100 °C and a true strain rate of $10s^{-1}$. The thin continuous line is a calculated result from the fitting equation, $\sigma = 106[1 - \exp(-8\epsilon)]^{0.38}$.

OUTPUTS

and

INTERACTIONS

SELECTED RECENT PUBLICATIONS*

1. Aftab, N.; Dutton, A.G.; Irving, A.D.; Lipman, N.; Clayton, B.R.; and Bond, L.J., Development of thermal condition monitoring techniques for composite wind turbine blades, Proceedings EWEC '91.

2. Balzar, D.; Ledbetter, H.; Roshko, A., Stacking Faults and Microstrain in $La_{1.85}M_{0.15}CuO_4$ (M = Ca, Ba, Sr) by Analyzing X-ray Diffraction Line Broadening, Proc. M^2S-HTSC III, Physica C, forthcoming.

3. Balzar, D.; Ledbetter, H., Stacking Faults and Microstrain in $(La-M)_2CuO_4$, M = Ca, Ba, Sr, Applied Physics, submitted.

4. Balzar, D., Profile Fitting of X-Ray Diffraction Lines with a Fourier-Method Analysis, J. Appl. Crystallography, forthcoming.

5. Blake, R.J. and Bond, L.J., Rayleigh wave scattering from 3-D surface slots, Review of Progress in Quantitative NDE, Vol. 10A, Ed. D.O. Thompson and D.E. Chementi, Plenum Publishing (New York), pp. 113–119.

6. Blake, R.J. and Bond, L.J., Rayleigh wave scattering from surface features: up steps and troughs, Ultrasonics, submitted.

7. Blake, R.J. and Bond, L.J., Rayleigh wave scattering from semi-circular depressions, Ultrasonics International '91, France, Butterworth-Heinemann (Guildford), in press.

8. Bond, L.J.; Zhu, H.; and Albach, P.H., Experimental examination of mode-conversion at hemispherical surface indentations, Ultrasonics, submitted.

9. Bond, L.J.; Chiang, C-H.; and Fortunko, C.M., Absorption of ultrasonic waves at high frequencies (10–20 MHz), Journal Acoustical Society of America, submitted.

10. Bond, L.J.; Aftab, N.; Clayton, B.R.; Dutton, A.G.; Irving, A.D.; and Lipman, N., Condition monitoring techniques for composite wind turbine blades, Review of Progress in Quantitative NDE, Vol. 11, Ed. D.O. Thompson and D.E. Chimenti, Plenum Publishing (New York), July, Brunswick, ME, in press.

---

*Papers that were published or accepted for publication by the Editorial Review Boards of NIST during fiscal year 1991.

11. Bond, L.J.; Yang, J., Ultrasonic Techniques for Sizing Voids by Using Area Functions, IEEE Proc., Part A, submitted.

12. Bond, L.J.; Taylor, J., Interaction of Rayleigh Waves with a Rib Attached to a Plate, Ultrasonics, Vol. 29 (5), pp. 451–458.

13. Bond, L.J. and Clark, R., Correspondence: Response of horizontal axis eddy current coils to layered media: a theoretical and experimental study, IEEE Proceedings, Part A, Vol. 138 (4), p. 248.

14. Bussiba, A.; Tobler, R.L.; Berger, J.R., Superconductor Conduits: Fatigue Crack Growth Rate and Near Threshold Behavior of Three Alloys, Adv. Cryo. Eng., Vol. 38, 1991, in press.

15. Cheng, Y.-W.; Tomer, A., Continuous-Cooling Transformation Characteristics and High-Temperature Flow Behavior of a Microalloyed SAE 1141 Steel, NISTIR 3964, 1991.

16. Cheng, Y.-W.; Kuziak, R.M., Microstructural Evolution in Microalloyed Forging Steels during Thermomechanical Processing, to be published in the Proceedings of the International Conference on Processing, Microstructure and Properties of Microalloyed and Other Modern High Strength Low Alloy Steels, June 3–6, 1991, Pittsburgh, PA.

17. Cheng, Y.W., The Continuous-Cooling-Transformation Diagrams of a Nb-Treated Bar Steel, to be published in the Proceedings of the International Conference on Processing, Microstructure and Properties of Microalloyed and Other Modern High Strength Low Alloy Steels, June 3–6, 1991, Pittsburgh, PA.

18. Clark, A.V.; Thompson, R.B.; Li, Y.; Reno, R.C.; Blessing, G.V.; Mitrakovic, D.V.; Schramm, R.E.; Matlock, D., Ultrasonic Measurement of Sheet Steel Texture and Formability: Comparison with Neutron Diffraction and Mechanical Measurements, Research in Nondestructive Evaluation, 2, 1990, pp. 239–257.

19. Clark, A.V., Progress towards Nondestructive, On-Line Measurement of Sheet Metal Formability, SAE Special Technical Publication, 865, Soc. Auto. Eng., Warrendale, PA (1991), pp. 1–14.

20. Datta, S.; Ledbetter, H.; Lei, M., Elastic Properties of Uniaxial-Fiber Reinforced Composites; General Features, Chapter in: Nondestructive Evaluation and Material Properties of Advanced Materials, New York: AIME, forthcoming.

21. Datta, S.; Ledbetter, H.; Taya, M., Elastic constants of SiC_w/Al_2O_3 composites: Measurements and modeling, to be submitted.

22. Dutton, A.G.; Aftab, N.; Bond, L.J.; Clayton, B.R.; Irving, A.D.; and Lipman, N., Infra red condition monitoring techniques for composite wind turbine blades, Proceedings BWEA, Swansea, UK.

23. Foldeaki, M.; Ledbetter, H.; Uggowitzer, P., Magnetic Properties of Cr—Mn Austenitic Stainless Steels, J. Magnetism Magn. Mater., submitted.

24. Foldeaki, M.; Ledbetter, H., Magnetic-Susceptibility-Temperature Peaks in Fe—Cr—Ni Alloys, Phil. Mag., submitted.

25. Foldeaki, M.; Ledbetter, H., Magnetic Susceptibility of Pr_2CuO_4 Monocrystals and Polycrystals: Field and Temperature Dependences, J. Appl. Phys., forthcoming.

26. Foldeaki, M.; Ledbetter, H.; Hidaka, Y., Magnetic Studies of $Pr_{2-x}Ce_xCu_{4-\delta}$, Proc. M^2S-HTSC III, Physica C, forthcoming.

27. Fortunko, C.M.; Renken, M.C.; Bratton, R.L.; Datta, S.K., Experiment and Modeling of Air-Coupled Ultrasonic Excitation of Plate Waves, Canadian Congress of Applied Mechanics, 1990, in press.

28. Fortunko, C.M.; Renken, M.C.; Murray, A., Examination of Objects Made of Wood Using Air-Coupled Ultrasound, Proc. 1990 IEEE Ultrasonics Symp. 1, B.R. McAvoy Ed. (IEEE, New York, 1991) pp. 1099—1103.

29. Heald, P.R.; Madigan, R.B.; Siewert, T.A.; Liu, S., Characterization of Spray Transfer in GMAW Using Through-the-Arc Sending, NISTIR 3976, 1991.

30. Heald, P.R.; Madigan, R.B.; Siewert, T.A.; Liu, S., Mapping the Droplet Transfer Modes for an ER 100S-1 GMAW Electrode, Welding Journal, submitted.

31. Hughes, G. and Bond, L.J., Leaky Rayleigh wave inspection under surface layers, Review of Progress in Quantitative NDE, Vol. 10B, Ed. D.O. Thompson and D. Chementi, Plenum Publishing (New York), pp. 1875—1882, 1991.

32. Kotecki, D.J.; Siewert, T.A., Constitution Diagram for Stainless Steel Welds Metals: A Modification of the WRC-1988 Diagram, Welding Journal, submitted.

33. Ledbetter, H., Thermal expansion and elastic constants, Int. J. Thermophys. 12 (1991) 637—642.

34. Ledbetter, H.; Austin, M., Thermal expansion of an SiC particle-reinforced aluminum composite, Int. J. Thermophys. 12 (1991) 731–739.

35. Ledbetter, H.; Kim, S.; Roshko, A., Critical-Temperature/Debye-Temperature Correlation in $(La–M)_2CuO_4$ Superconductors, Proc. Chem-HTSC, Physica C, forthcoming.

36. Ledbetter, H.; Lei, M., Elastic Constants of Fiber-Reinforced Composites: A Fresh Measurement Approach, IEEE 1990 Ultrasonics Symposium Proceedings (IEEE, New York, 1990) 1267–1269.

37. Ledbetter, H.; Lei, M., Estimated dT_c/dP and $dT_c/d\sigma_{ij}$ for the $Y_1B_2Cu_3O_7$ Superconductor, Physica C 177 (1991) 86–88.

38. Ledbetter, H.; Lei, M., Monocrystal Elastic Constants of Orthotropic $Y_1Ba_2Cu_3O_7$; An Estimate, J. Mater. Res., forthcoming.

39. Ledbetter, H.; Kim, S.; Togano, K., Elastic Properties of $Bi_2Sr_2Ca_1Cu_2O_8$ and $Bi_2Sr_{1.5}Ca_{1.5}Cu_2O_8$, Proc. M^2S-HTSC III; Physica C, forthcoming.

40. Ledbetter, H.; Datta, S.; Kriz, R., Elastic Constants of a $\gamma–Al_2O_3–SiO_2$ (Fiber)/PEEK Composite: Measurements, Modeling, and Low Temperature, J. Appl. Phys., submitted.

41. Ledbetter, H.; Fortunko, C.M.; Lin, S., Group and Phase Sound Velocities in an $Eu_1Ba_2Cu_3O_7$ Superconductor and Related Oxides, IEEE 1990 Ultrasonics Symposium Proceedings (IEEE, New York, 1990) 1215–1219.

42. Ledbetter, H., Atomic Frequency and Elastic Constants, Z. Metallk., forthcoming.

43. Ledbetter, H.; Kim, S.; Roshko, A., Correlation between T_c and Elastic Constants of $(La–M)_2CuO_4$, M = Ca, Ba, Sr, Z. Physik B: Condensed Matter, submitted.

44. Ledbetter, H., Elastic Constants of Polycrystalline $Y_1Ba_2Cu_3O_x$, J. Mater. Res., submitted.

45. Ledbetter, H.; Datta, S., Elastic Constants of a Tungsten-Particle Copper-Matrix Composite, JMSE Int. J. 34 (1991) 194–197.

46. Ledbetter, H.; Datta, S.; Kriz, R., Elastic constants of an Al_2O_3 (fiber)/PEEK composite: Measurements, modeling, and low temperatures, to be submitted.

47. Lei, M.; Ledbetter, H., Oxides and Oxide Superconductors: Elastic and Related Properties, NIST TN 1349 (1991), forthcoming.

48. Lin, S.; Lei, M.; Ledbetter, H., Elastic Constants and Debye Temperature of $Y_1Ba_2Cu_3O_x$: Effect of Oxygen Content, to be submitted.

49. Masuda-Jindo, K.; Tewary, V.K.; Thomson, R.M., Atomic Theory of Fracture of Brittle Materials: Application to Covalent Semiconductors, Journal of Materials Research, Vol. 6, p. 1553–1566 (1991).

50. McColskey, J.D.; Reed, R.P.; Simon, N.J.; Bransford, J.W., Recommended Changes in ASTM Test Methods D2512-82 and G86-84 for Oxygen-Compatibility Mechanical Impact Tests, Flammability and Sensitivity of Materials in Oxygen-Enriched Atmospheres, Joel Stoltzfus, ed., ASTM STP 1111, American Society for Testing and Materials, 1991.

51. McHenry, H.I., Materials Science and Engineering Laboratory, Materials Reliability Division Technical Activities 1990, NISTIR 4395.

52. McHenry, H.I., A Proposed National High-Performance Structural Materials Program; Part 2: High-Performance Steel, Proc., CERF Project on High-Performance Concrete and Steel Planning Meeting, Washington, DC, 8/20–22, 1991.

53. Nakajima, H.; Yoshida, K.; Tsuji, H.; Tobler, R.L.; Hwang, I.; Morra, M.; Ballinger, R.G., The Charpy Impact Test as an Evaluation of 4 K Fracture Toughness, Adv. Cryo. Eng., Vol. 38, 1991, in press.

54. Peterson, G.L.; Chick, B.B.; Fortunko, C.M., A Versatile Ultrasonic Measurement System for Flaw Detection and Material Property Characterization in Composite Materials, Proc., 1991 Iketari Conf. on NDE, Japan, in press.

55. Purtscher, P.T.; McColskey, J.D.; Drexler, E.S., Aluminum-Lithium Alloys: Evaluation of Fracture Toughness by Two Test Standards, ASTM E813 and E1304, to be submitted.

56. Purtscher, P.T.; Drexler, E.S., Through-Thickness Mechanical Properties of High-Strength Aluminum alloy Plates for Cryogenic Applications, Proc., TMS Meeting on Lightweight Alloys for Aerospace Applications, submitted.

57. Purtscher, P.T., Quantifying the Embrittlement due to Sensitization in an Austenitic Stainless Steel, Scripta Metallurgica et Materialia, submitted.

58. Read, D.T.; Lucey, G.K., Automated Finite Element Mesh Generation for SMT Solder Joints, J. Electronic Packaging, submitted.

59. Read, D.T.; Pfuff, M., Potential drop in the center-cracked panel with asymmetric crack extension, Int. J. Fracture, submitted.

60. Reed, R.P.; Purtscher, P.T.; Simon, N.J.; McColskey, J.D.; Walsh, R.P.; Berger, J.R.; Drexler, E.S.; Santoyo, R.L.; Aluminum Alloys for ALS Cryogenic Tanks: Comparative Measurements of Cryogenic Mechanical Properties of Al–Li Alloys and Alloy 2219, NISTIR 3979, 1991.

61. Reed, R.P.; McCowan, C.N.; Simon, N.J.; McColskey, J.D., Deformation and Fracture Characteristics of Al–Li Alloys in LOX Mechanical-Impact Tests, Adv. Cryo. Eng.-Mater., Vol. 38, in press.

62. Reed, R.P.; Simon, N.J.; McColskey, J.D.; Berger, J.R.; McCowan, C.N.; Bransford, J.W.; Drexler, E.S.; Walsh, R.P., Aluminum Alloys for ALS Cryogenic Tanks: Oxygen Compatibility, Volume 1, AL-TR-90-063, Astronautics Laboratory, Edwards AFB, CA (1990).

63. Reed, R.P.; Simon, N.J.; McColskey, J.D.; McCowan, C.N.; Drexler, E.S., Aluminum Alloys for ALS Cryogenic Tanks: Oxygen Compatibility, Volume 2, AL-TR-90-063, Astronautics Laboratory, Edwards AFB, CA (1990).

64. Reed, R.P.; McCowan, C.N.; McColskey, J.D.; Simon, N.J.; Macro- and Microreactions in Mechanical-Impact Tests of Aluminum Alloys, Flammability and Sensitivity of Materials in Oxygen-Enriched Atmospheres: 5th Vol., ASTM STP 1111, J.M. Stoltzfus, ed., Phil., PA (1991), pp. 240–259.

65. Reed, R.P.; Simon, N.J.; Berger, J.R.; McColskey, J.D.; Influence of Specimen Absorbed Energy in LOX Mechanical-Impact Tests, Flammability and Sensitivity of Materials in Oxygen-Enriched Atmospheres, 5th Vol., ASTM STP 1111, J.D. Stoltzfus, ed., Phila., PA (1991), pp. 381–398.

66. Schramm, R.E.; Clark, A.V.; Mitrakovic, D.V.; Schaps, S.R., Ultrasonic Measurements of Residual Stress in Railroad Wheels, Proc., Practical Applications of Residual Stress Technology Conf., ASM Intl., May 1991.

67. Schramm, R.E.; Clark, A.V.; Mitrakovic, D.V.; Cohen, Y.; Shull, P.J.; Schaps, S.R., Report No. 22, Tread Crack Detection in Railroad Wheels: An Ultrasonic System Using EMATs, NISTIR 3967, May 1991.

68. Schramm, R.E.; Clark, A.V.; Mitrakovic, D.V.; Schaps, S.R., McGuire, T.J., Report No. 23, Residual Stress Detection in Railroad Wheels: An Ultrasonic System Using EMATs, NISTIR 3968, May 1991.

69. Schramm, R.E.; Clark, A.V.; Mitrakovic, D.V.; Schaps, S.R., Residual Stress by Ultrasound: Railroad Wheel Rims, Proceedings Sixth International Fracture Mechanics Summer School, Novi Sad, Yugoslavia, June 1991.

70. Shiloh, K.; Som, A.K.; and Bond, L.J., Characterization of high frequency focused ultrasonic transducers using modulation transfer functions, IEEE Proceedings, Part A, Vol. 138 (4) pp. 205–212.

71. Shiloh, K.; Bond, L.J.; and Som, A.K., Detection limits for single small flaws and groups of flaws when using focused ultrasonic transducers, Ultrasonics, submitted.

72. Siewert, T.A., Measurement of Hydrogen in Welds, Proc., 6th Intl. Fracture Mechanics Summer School, June 1991, Novi Sad, Yugoslavia.

73. Siewert, T.A.; Gerken, J.M., Welding Technology in Eastern Europe, Welding Journal, 70, p. 49, March 1991.

74. Siewert, T.A.; Austin, M.W.; Lucey, G.; Plott, M., System Evaluation and Qualification Standards for an X-Ray Laminography System, Proceedings of the Technical Program, NEPCON-East, June 10 to 13, 1991, Boston, Massachusetts, p. 51, 1991.

75. Siewert, T.A., Report of 1991 Actions by the International Institute of Welding, Materials Evaluation 49, p. 470, April 1991.

76. Siewert, T.A.; McCowan, C.N., Joining of Austenitic Stainless Steels for Cryogenic Applications, Advances in Cryogenic Engineering – Metals, submitted.

77. Siewert, T.A.; Fitting, D.W.; Austin, M.W., A Rotationally Symmetric Image Quality Indicator for Digital X-Ray Imaging Systems, Materials Evaluation, submitted.

78. Siewert, T.A.; Tomer, A., Microstructure, Composition, and Hardness of Rockwell C Hardness Blocks, NISTIR 91-3960, 1991.

79. Siewert, T.A., U.S. May Have to Change its Standards to Capitalize on Future Trade Opportunities, American Machinist, 135, Number 5, p. 27, May 1991.

80. Siewert, T. A.; McCowan, C. N.; Olson, D. L., Ferrite number prediction for stainless steel welds, Chapter in book published by American Society for Metals, in press.

81. Siewert, T.A.; McCowan, C.N., Development of an SMA Electrode to Match Type 316 LN Base Metal Cryogenic Properties, Cryogenics, forthcoming.

82. Siewert, T.A., Standard Formats for Welding Property Data, Proceedings of Computerization of Welding Conference III, Ypsilanti, MI, September 12–14, 1990, in press.

83. Siewert, T.A. and Austin, M.W., An X-ray Image Quality Indicator Designed for Easy Alignment, International Institute of Welding Document V-965-91, American Secretariat: American Welding Society, Miami, Florida, 1991.

84. Siewert, T.A. and Madigan, R.B., Arc Sensor Module for the Programmable Automated Welding System, Report to David Taylor Research Center under Contract N00167-90-WR-00204, 1991.

85. Simon, N.J.; Reed, R.P.; Walsh, R.P., Compression and Shear Tests on Vacuum-Impregnated Composites at Cryogenic Temperatures, Adv. Cryo. Eng. (Mater.), Vol. 38, 1992.

86. Simon, N.J.; Drexler, E.S.; Reed, R.P., Review of Cryogenic Mechanical and Thermal Properties of Al–Li Alloys and Alloy 2219, NISTIR 3971, 1991.

87. Simon, N.J.; Reed, R.P., Temperature Increases in Aluminum Alloys During Mechanical-Impact Tests for Oxygen Compatibility, Flammability and Sensitivity of Materials in Oxygen Enriched Atmospheres: Vol. 5, ASTM STP 1111, J.M. Stoltzfus and K. McIlroy, Eds., Amer. Soc. for Testing and Mater., Phil., 1991.

88. Simon, N.J.; McColskey, J.D.; Reed, R.P.; Garcia-Salcedo, C.M., Reaction Sensitivities of Al–Li Alloys and Alloy 2219 in Mechanical-Impact Tests, Flammability and Sensitivity of Materials in Oxygen-Enriched Atmospheres: Vol. 5, ASTM STP 1111. Joel M. Stolzfus and K. McIlroy, Eds., Amer. Soc. for Testing and Mater., Phil., 1991.

89. Simon, N.J.; Drexler, E.S.; Reed, R.P., Review of Cryogenic Mechanical and Thermal Properties of Al–Li Alloys and Alloy 2219, Final Report for the period Nov. 1988 to Jun, 1990, Air Force Astronautics Lab., AL-TR-90-064, Sept. 1990.

90. Som, A.K.; Bond, L.J.; and Taylor, K.J., Characterization of diffusion bonds using an acoustic microscope, Review of Progress in Quantitative NDE, Vol. 10B, Ed. D.O. Thompson and D. Chimenti, Plenum Publishing (New York), pp. 1391–1398.

91. Szanto, M.; Read, D.T., Application of the J-Integral to Stress-Strain Concentrations, Engineering Fracture Mechanics, submitted.

92. Tewary, V.K.; Fortunko, C.M., A Computationally Efficient Representation for Elastic Wave Propagation in Anisotropic Solids, J. Acoust. Soc. Amer., submitted.

93. Tewary, V.K., Elastic Green's Function for a Bimaterial Composite Solid Containing a Free Surface Normal to the Interface, J. Mater. Res. (to be published in Dec. 1991).

94. Tewary, V.K., Green's Function for Generalized Hilbert Problem for Cracks and Free Surfaces in Composite Materials, J. Mater. Res. (to be published in Dec. 1991).

95. Tewary, V.K.; Kriz, R.D., Generalized Plane Strain Analysis of a Bimaterial Composite Containing a Free Surface Normal to the Interface, J. Mater. Res. (to be published in Dec. 1991).

96. Tewary, V.K.; Kriz, R.D., Stress Distribution in a Bimaterial Composite Containing a Free Surface, Modern Theory of Anisotropic Elasticity and Applications, Editor T.C.T. Ting (publisher SIAM, Philadelphia), forthcoming.

97. Tewary, V.K.; Heyliger, P.R.; Clark, A.V., Theory of Capacitive Probe Method for Noncontact Characterization of Dielectric Properties of Materials, Journal of Materials Research, Vol. 6, p. 629–638 (1991).

98. Tewary, V.K. and Fortunko, C.M., Application of Time Dependent Green's Function Method to Scattering of Elastic Waves in Anisotropic Solids, Review of Progress in Quantitative Nondestructive Evaluation, Vol. 10 B, (edited by D.O. Thompson and D.E. Chimenti; Plenum Press, NY) p. 1415 (1991).

99. Tewary, V.K. and Thomson, R.M., Lattice Statics of Interfaces and Interfacial Cracks in Bimaterial Solids, Journal of Materials Research, submitted.

100. Tobler, R.L.; Ma, L.M.; Reed, R.P., Mechanical Properties and Warm Prestress of Ultra-Low Carbon Steel at 4 K, Proc., Intl. Industrial Symp. on the Super Collider, in press.

101. Tobler, R.L.; Bussiba, A.; Guzzo, J.F.; Hwang, I.S., Charpy Specimen Tests at 4 K, Adv. Cryo. Eng., Vol. 38, 1991, in press.

102. Tobler, R.L.; Berger, J.R.; Bussiba, A., Long-Crack Fatigue Thresholds and Short Crack Simulation at Liquid Helium Temperature, Adv. Cryo. Eng., Vol. 38, 1991, in press.

103. Tobler, R.L.; Shimada, M., Warm Precracking at 295 K and its Effects on the 4-K Toughness of Austenitic Steels, ASTM Journal of Testing and Evaluation, Vol. 19, No. 4, July 1991, pp. 312–320.

104. Tobler, R.L.; Reed, R.P.; Hwang, I.S.; Morra, M.M.; Ballinger, R.G.; Nakajima, H.; Shimamoto, S., Charpy Impact Tests near Absolute Zero, Journal of Testing and Evaluation, Vol. 19, No. 1, Jan. 1991, pp. 34–40.

105. Walsh, R.P.; Reed, R.P.; McColskey, J.D.; Fehringer, W.; Berger, J.R., A Cryogenic 4.4 MN Mechanical Test System for Full-Scale Tests of Composite Support Struts, NISTIR B91-0161.

106. Walsh, R.P.; Reed, R.P.; McColskey, J.D., Large Scale Tests of Composite Support Struts for Superconducting Magnetic Energy Storage Rings, Adv. Cryogenic Engineering, Vol. 38, 1991, in press.

107. Yang, J. and Bond, L.J., Reconstruction of volumetric voids using ultrasonic backscattering response, Ultrasonics International '91, France, Butterworth-Heinemann (Guildford), in press.

108. Yang, J. and Bond, L.J., Ultrasonic sizing of voids using area functions, Review of Progress in Quantitative NDE, Vol. 11, Ed D.O. Thompson and D.E. Chimenti, Plenum Publishing (New York), July, Brunswick, ME, in press.

109. Zhu, H.; Bond, L.J.; and Albach, P.H., Experimental investigation of Rayleigh wave generation at a surface pit with compression wave incidence, Ultrasonics International '91, France, Butterworth-Heinemann (Guildford), in press.

SELECTED TECHNICAL AND PROFESSIONAL COMMITTEE LEADERSHIP

American Society for Testing and Materials
- E07.01: Nondestructive Evaluation
  - Task Force on Evaluation of Real-Time Systems
    - T. A. Siewert, Member
- E28.07: Impact Testing
  - T. A. Siewert, Chairman
- E28.10.02: Temperature Effects
  - R.L. Tobler, Task Group Leader

American Welding Society
- Technical Papers Committee
  - T. A. Siewert
- Welding Journal
  - H. I. McHenry, Reviewer
  - T. A. Siewert, Reviewer
- Conference on Computerization of Welding Data
  - Organizing Committee
    - T. A. Siewert

International Institute of Welding
- Task Group for Elastic—Plastic Fracture-Mechanics Standard
  - D. T. Read
- Commission V on Nondestructive Evaluation
  - T.A. Siewert

International Union of Theoretical and Applied Mechanics
- Organizing Committee
  - H. M. Ledbetter

Metallurgical Society
- Metallurgical Transactions
  - H. M. Ledbetter

Welding Research Council
- Data Base Task Group
  - T. A. Siewert
- Materials and Welding Procedures Subcommittee
  - T. A. Siewert
- University Research Committee
  - T. A. Siewert

AWARDS

Materials Reliability Division staff received the following awards in 1991:

Bronze Medals

Thomas Siewert	For developing a materials research program that contributes to the quality, reliability, and safety of welded structures.
David Read	For developing a fracture mechanics approach to assessing the reliability of electronic packages.

Safety Award

Daniel Vigliotti	For leadership of the safety program in the Materials Reliability Division (1991).

Measurement Service Award

Dominique Shepherd Thomas Siewert Daniel Vigliotti	For successful implementation of the certification program for Charpy impact test machines (1991).

INDUSTRIAL AND ACADEMIC INTERACTIONS

Industrial Interactions

AC Rochester

The Welding Group is hosting a research associate from this division of General Motors. He is studying our welding arc sensor technology for application on their production lines.

Alcoa

The Cryogenic Materials Group is collaborating with Alcoa to evaluate the metallurgical and mechanical properties of Al–Li alloys.

Bechtel

The Cryogenic Materials Group is conducting large-scale tests on composite materials for use in the superconducting magnetic energy storage system.

Chaparral Steel

Yi-Wen Cheng and Dominique Shepherd are working with Chaparral Steel to determine the influence of processing on the mechanical properties of new microalloyed bar steels.

Chrysler Corporation

Yi-Wen Cheng is working with Chrysler Motors Corporation to develop the metallurgical data needed for the direct forging of microalloyed bar steels.

Comalco (Melbourne)

H. Ledbetter collaborates with M. Lee on the elastic constants of Al_2O_3/Al composites.

Composite Technology Development, Inc.

N.J. Simon and others in the Cryogenics Materials Group are developing new test methods and screening radiation-resistant insulation for superconducting magnets.

Conoco

D.T. Read is working with Conoco to develop fiber optic techniques to detect damage in uniaxial composite rods being evaluated for use as tendons in tension-leg platforms.

Eaton Corporation

Yi-Wen Cheng is working with Eaton to develop the metallurgical data needed for the direct forging of microalloyed bar steels.

Ford Motor Company

A. V. Clark is working with Ford on the simulation of ultrasonic measurement of formability in a continuous annealing line.

General Atomics

The Cryogenic Materials Group is conducting large-scale tests on composite materials for use in the superconducting magnetic energy storage system.

General Electric

T. A. Siewert is working with the Aircraft Engines Department of General Electric and the Army Materials Technology Laboratory to develop a military standard for radioscopic inspection.

Hercules

D.W. Fitting and C.M. Fortunko are working with Hercules on ultrasonic techniques for nondestructive evaluation of composites.

Hitachi (Japan)

H. Ledbetter collaborates with H. Tsuiki on elastic constants of Bi—O monocrystal superconductors.

International Copper Association, Ltd.

N.J. Simon and E. S. Drexler are cooperating with ICA to develop the database for copper and producing a monograph describing the cryogenic properties.

Kobe Steel, Ltd.

R.L. Tobler is collaborating with M. Shimada in studies of mechanical test variables affecting the measurement of fracture mechanics parameters for steels at liquid helium temperature.

Lockheed

C. M. Fortunko is working with Lockheed to develop a new standard test block to calibrate transducers used to inspect composite materials.

Lukens Steel

Yi-Wen Cheng and Harry McHenry are working with Lukens Steel to qualify thermomechanically processed steels for use in Naval shipbuilding.

Martin-Marietta

The Cryogenic Materials Group is generating and compiling mechanical property data on a new Al–Li alloy.

McDonnell–Douglas

J. D. McColskey is measuring the mechanical properties of graphite/PEEK composites, which may be used on the national aerospace plane (NASP).

Minnesota Valley Engineering

R.L. Tobler collaborated with J.F. Guzzo to develop and validate an improved 4-K Charpy impact test procedure suitable for industrial testing machines and purposes.

Omega Marine International

J.D. McColskey participates on the Joint Industrial Program to evaluate the prospects of using aramid rope as mooring line for deepwater, offshore oil well platforms.

Precision Acoustic Devices (PAD), Inc.

C. M. Fortunko is collaborating with PAD in the development of an air-coupled ultrasonic instrument for the nondestructive evaluation of composite materials.

NTT (Japan)

H. Ledbetter collaborates with Y. Hidaka on oxide-superconductor elastic constants.

H. Ledbetter collaborates with K. Kimoshita on oxide-superconductor elastic constants.

Reynolds Metals

The Cryogenic Materials Group is collaborating with Reynolds to evaluate the metallurgical and mechanical properties of Al–Li alloys.

Torrington Company

Yi-Wen Cheng is working with Torrington Company to develop high-temperature, high-strain rate flow properties of bearing steels.

Union Pacific Railroad

R. E. Schramm is developing an instrument to embed in railroad track to be used for the roll-by inspection of wheels.

Welding Research Council

T. A. Siewert and D. P. Vigliotti evaluate welded samples for the Materials and Welding Procedures Committee as part of the WRC effort to develop prequalified welding procedures. The committee is composed of welding fabricators, inspection agencies, insurance companies, sheet-metal workers, and other representatives of the welding industry.

Westmoreland Testing and Research Corporation

The Cryogenic Materials Group advises this company in the design and construction of cryogenic apparatus for the transfer of cryogenic mechanical testing technology to industry.

Academic Interactions

Atominstitut der Osterreichen Universitaten, Vienna

N.J. Simon cooperates with H.W. Weber in studies of the properties of irradiated composites and activation of structural alloys for fusion reactors.

Colorado School of Mines

T.A. Siewert is an Adjunct Professor of Metallurgy

T. A. Siewert is working with S. Liu in the study of droplet transfer in the welding arc.

A. V. Clark collaborates with D. Matlock on texture and formability research using ultrasonics.

P.T. Purtscher works with Drs. G. Krauss and D. Matlock on the characterization of the mechanical properties of austenitic stainless steels.

Colorado State University

H. Ledbetter collaborates with P. Heyliger (Civil Engineering) in studying the natural resonance of regular solids.

Davidson College

H. Ledbetter collaborates with L. Cain (Physics) on austenitic-steel elastic constants.

Harvard University

I.-H. Lin completed a one-year sabbatical to study the fracture and deformation of electronic materials under the direction of Professor J.R. Rice.

Indian Institute of Technology (Madras)

H. Ledbetter collaborates with R. Rao (Physics) on higher-order elastic constants.

Institute of Metal Research (Shenyang, P. R. China)

H. Ledbetter collaborates with Y. Li in studying austenitic-steel elastic constants.

Institute of Metallurgy, ETH (Zurich)

H. Ledbetter collaborates with P. Uggowitzer in studying austenitic-steel elastic constants and magnetic properties.

Iowa State University: Center for Advanced NDE, Ames Laboratories

A. V. Clark collaborates with R. B. Thompson on texture and formability using ultrasonics.

Massachusetts Institute of Technology

I.-H. Lin works with A. Argon in studying the brittle-to-ductile transition in cleavage fracture.

R.L. Tobler collaborates with Dr. I.S. Hwang of the Materials Sciences Department in the evaluation of nickel-base superconductor sheath alloys for applications at 4 K.

Max-Planck-Institut für Metallforschung (Stuttgart, Germany)

H. Ledbetter collaborates with M. Weller to study the internal friction and dielectric constants of various materials.

National Research Institute for Metals (Tsukuba, Japan)

H. Ledbetter collaborates with T. Ogata to study low-temperature elastic properties.

H. Ledbetter collaborates with K. Togano to study oxide-superconductor elastic constants.

R.L. Tobler works with K. Nagai to plan and execute international round-robin tests programs in support of cryogenic test standards.

Ohio State University

Vinod Tewary of Ohio State is a guest scientist working with C.M. Fortunko on modelling interface problems related to the fracture of composite materials.

Osaka University

H. Ledbetter collaborates with Y. Tsunoda (Physics) to study Cu(Fe) elastic constants.

A. V. Clark works with H. Fukuoka and M. Hirao on the development of ultrasonic measurement techniques for determining residual stress and texture.

Stanford University

A. V. Clark and S.R. Schaps collaborate with B. A. Auld on capacitive array research.

C. M. Fortunko is collaborating with Professor B. T. Kuri-Yakub on the development of air-coupled ultrasonic transducers.

J.D. McColskey collaborates with Dr. G. Springer in the development of optimum lay-up angles for maximizing the compressive axial strengths of E-glass—epoxy composite support tubes.

Technischen Universitat, Munich

N.J. Simon and others of the Cryogenic Materials Group cooperate with H. Gerstenberg to develop in-situ 4-K shear—compression tests for superconducting magnet insulation after irradiation at the Munich Research Reactor.

Tohoku University

H. Ledbetter collaborates with Y. Shindo (Materials Processing Department) on waves in composites.

H. Ledbetter collaborates with M. Taya (Materials Processing Department) on composite-material elastic constants.

R.L. Tobler interacts with Dr. H. Takahashi of the Research Institute for Fracture Technology to document fracture mechanics test procedures for structural alloys at 4 K.

Tsinghua University (P.R. China)

H. Ledbetter continues studies with Y. He (Physics) on oxide-superconductor elastic constants.

University of Arkansas

H. Ledbetter collaborates with Z. Zheng (Physics Department) on oxide-superconductor elastic constants.

University of Belgrade

D. Mitraković was a guest researcher at NIST in the Nondestructive Evaluation group, working on instrumentation for inspecting railroad wheels.

University of California

H. Ledbetter collaborates with R. Fisher in studying oxide-superconductor specific heats.

University of Colorado

H. Ledbetter is an Adjunct Professor in the Department of Mechanical Engineering.

H. Ledbetter collaborates with Professor A. Hermann (Physics) on oxide-superconductor elastic constants.

University of Connecticut

H. Ledbetter collaborates with S. Datta (Mechanical Engineering) on problems of waves in composites.

University of Geneva

H. Ledbetter continues studies with B. Seeber on the elastic constants of Chevrel-phase superconductors.

University of Hawaii

H. Ledbetter collaborates with M. Manghnani (Geophysics) to study pressure dependence of elastic constants of oxide superconductors.

University of Maryland

H. Ledbetter collaborates with R. Reno (Physics) on studies of the effects of texture on elastic constants.

Professor J.W. Dally is working at NIST with D.T. Read on high resolution experimental mechanics while on sabbatical leave for the 1991-92 academic year.

University of Michigan

D.W. Fitting is collaborating with researchers at the University of Michigan on the development of silicon-based acoustical arrays.

University of South Carolina

H. Ledbetter collaborates with T. Datta (Physics) on magnetic properties: steels and superconductors.

University of Stuttgart

H. Ledbetter collaborates with B. Gairola (Institute for Theoretical and Applied Physics) on graphite-fiber elastic constants.

H. Ledbetter collaborates with E. Kröner (Institute for Theoretical and Applied Physics) on monocrystal–polycrystal elastic constants

University of Tsukuba

H. Ledbetter collaborates with T. Suzuki (Applied Physics) on elastic constants and phase transitions.

H. Ledbetter collaborates with K. Otsuka (Materials Science), on the elastic constants of the monocrystal shape-memory alloy Cu–Al–Ni.

H. Ledbetter collaborates with M. Saito (Engineering Mechanics), on elastic constants of technical solids.

H. Ledbetter collaborates with M. Uwe (Materials Science) on elastic properties of barium-bismuthate superconductors.

University of Zagreb

H. Ledbetter collaborates with D. Balzar (Metallurgy) on defect properties of oxide superconductors.

Virginia Polytechnic Institute and State University

J.D. McColskey collaborates with Dr. M. Hyer in analysis of structural composite support tubes for superconducting magnetic energy storage rings.

Yale University

H. Ledbetter collaborates with B. Adams (Mechanical Engineering on elastic-constants/texture relationships.

National Laboratories

Argonne

H. Ledbetter collaborates with B. Veal on defect properties of oxide superconductors.

Brookhaven

R.L. Tobler interacts with members of the Magnet Design Group to assist in evaluation of construction materials for the Superconducting Super Collider.

Instituto Metallurgia "G. Collonetti"

R.P. Walsh works with Drs. C. Ferrerro and F. Pavesi to execute interlaboratory tests designed to evaluate appropriate materials and techniques for cryogenic strain gaging at liquid helium temperature.

Japan Atomic Energy Research Institute (Tokai-mura, Japan)

R.L. Tobler collaborates with members of the Superconducting Machinery Laboratory to develop and validate cryogenic mechanical property test standards that are subsequently presented for adoption by the American Society for Testing and Materials and the Japanese Industrial Standards organizations.

Los Alamos

H. Ledbetter collaborates with M. Lei and A. Migliori on oxide-superconductor elastic constants.

National Research Institute for Metals (Tsukuba, Japan)

R.L. Tobler works with Drs. K. Nagai and T. Ogata to plan, execute, and publish prestandards research supporting the developing of mechanical test standards at liquid helium temperature.

Nuclear Research Centre (Negev, Israel)

R.L. Tobler works with A. Bussiba and others to develop improved fracture mechanics test procedures for structural alloys.

APPENDIX

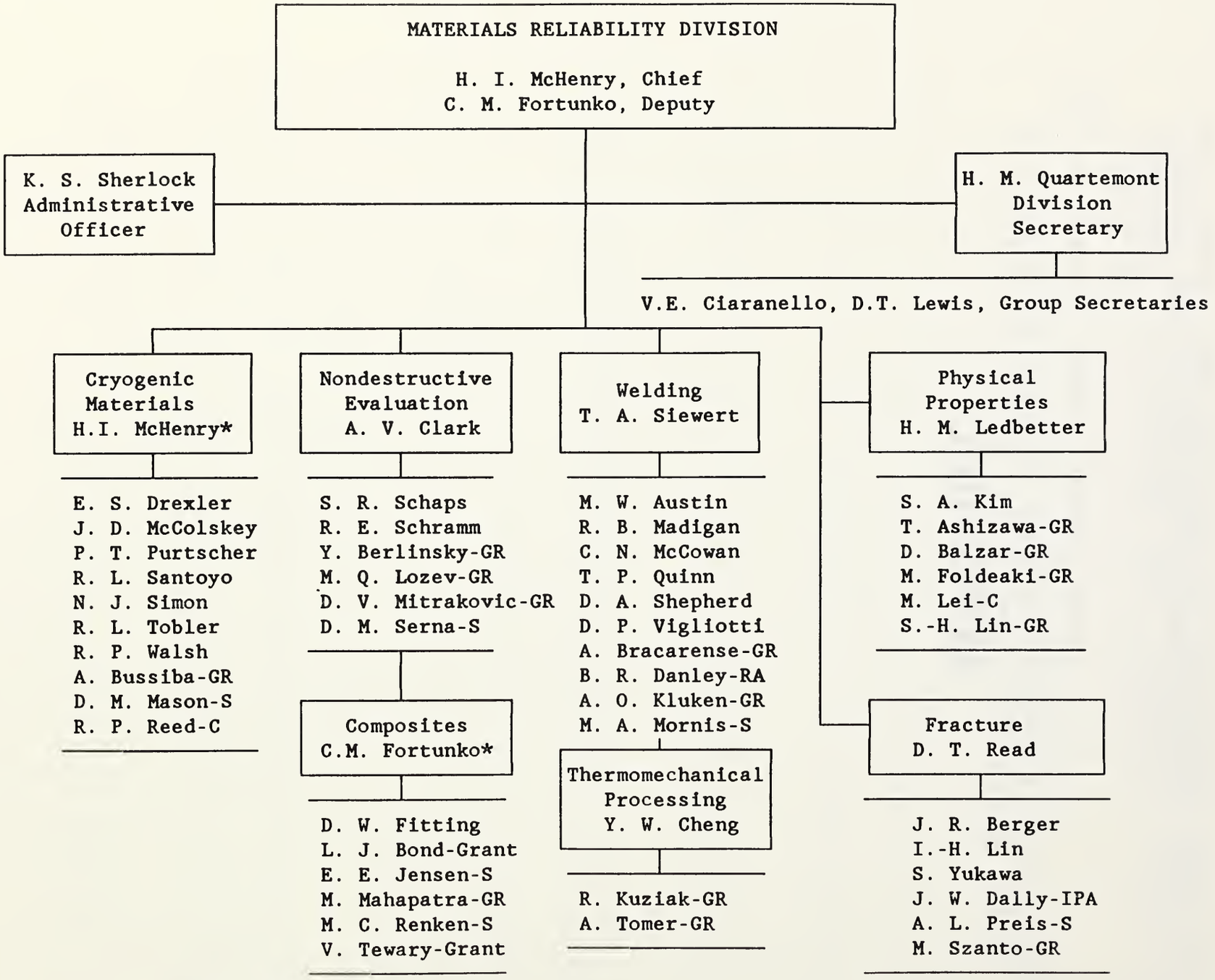

RA – Research Associate
GR – guest researcher
S – student
C – contract
* – Acting

U.S.DEPARTMENT OF COMMERCE
National Institute of Standards and Technology

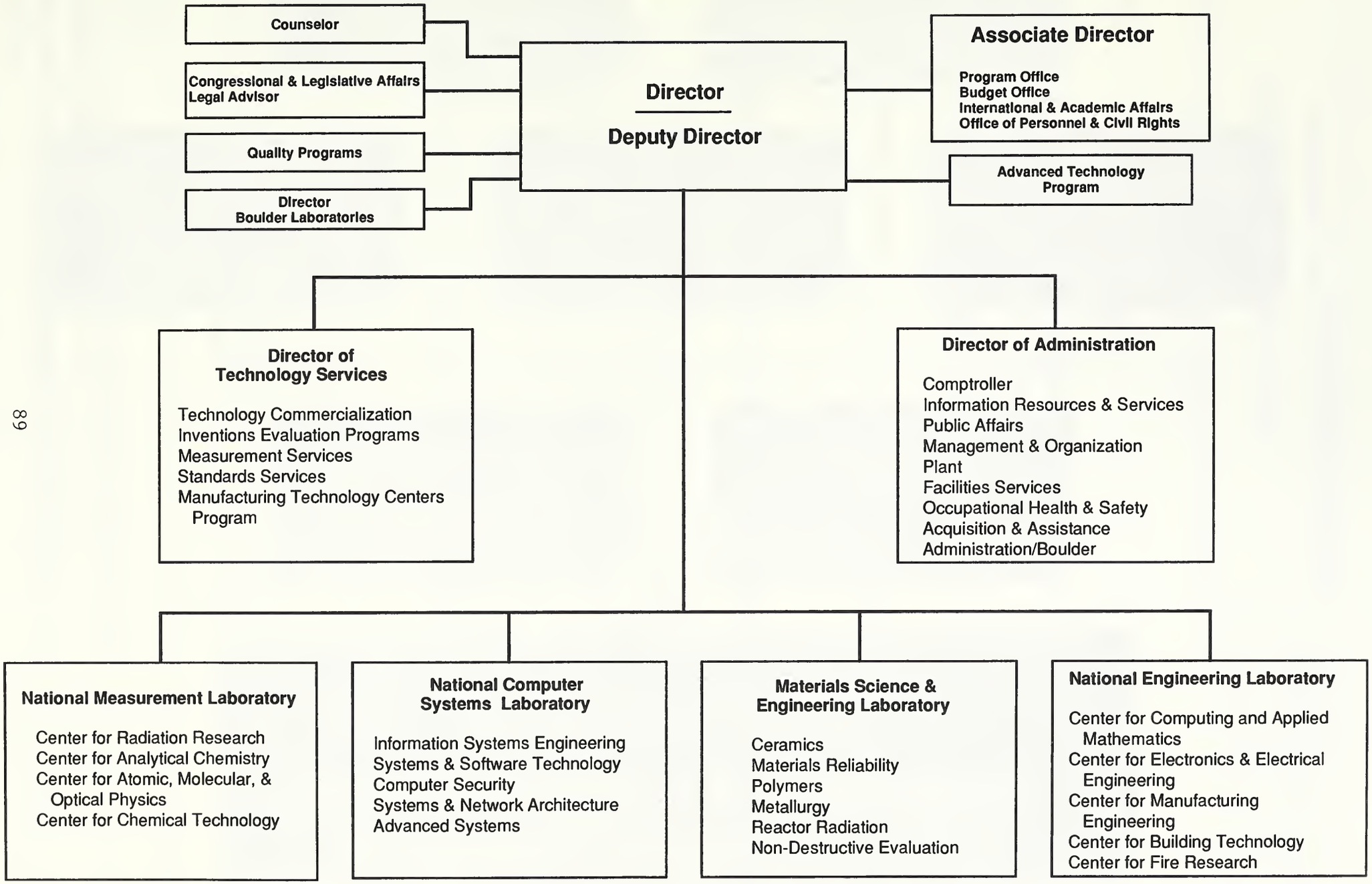

MATERIALS SCIENCE AND ENGINEERING LABORATORY

L.H. Schwartz, Director
H.L. Rook, Deputy Director

Nondestructive Evaluation

H.T. Yolken, Chief
J.P. Gudas, Deputy

Institute Scientists

J.W. Cahn
R.M. Thomson
S.M. Wiederhorn

Metallurgy

E.N. Pugh, Chief
S.C. Hardy, Deputy

Polymers

L.E. Smith Chief
B.M. Fanconi, Deputy

Ceramics

S.M. Hsu, Chief
S.J. Dapkunas, Deputy

Materials Reliability

H.I. McHenry, Chief
C.M. Fortunko, Deputy

Reactor Radiation

J.M. Rowe, Chief
T.M. Raby, Deputy

BL-114A
(5-90)

U.S. DEPARTMENT OF COMMERCE
NATIONAL INSTITUTE OF STANDARDS AND TECHNOLOGY

BIBLIOGRAPHIC DATA SHEET

1. PUBLICATION OR REPORT NUMBER
NISTIR 4695

2. PERFORMING ORGANIZATION REPORT NUMBER
B92-0031

3. PUBLICATION DATE
DECEMBER 1991

4. TITLE AND SUBTITLE
Materials Science and Engineering Laboratory
Materials Reliability Division
Technical Activities 1991

5. AUTHOR(S)
Harry I. McHenry, Editor

6. PERFORMING ORGANIZATION (IF JOINT OR OTHER THAN NIST, SEE INSTRUCTIONS)
U.S. DEPARTMENT OF COMMERCE
NATIONAL INSTITUTE OF STANDARDS AND TECHNOLOGY
BOULDER, COLORADO 80303-3328
EARLY ASSIGNMENT OF NISTIR 4695.

7. CONTRACT/GRANT NUMBER

8. TYPE OF REPORT AND PERIOD COVERED

9. SPONSORING ORGANIZATION NAME AND COMPLETE ADDRESS (STREET, CITY, STATE, ZIP)
Materials Reliability Division, 853
National Institute of Standards and Technology
325 Broadway
Boulder, CO 80303

10. SUPPLEMENTARY NOTES

11. ABSTRACT (A 200-WORD OR LESS FACTUAL SUMMARY OF MOST SIGNIFICANT INFORMATION. IF DOCUMENT INCLUDES A SIGNIFICANT BIBLIOGRAPHY OR LITERATURE SURVEY, MENTION IT HERE.)

This report describes the 1991 fiscal-year programs of the Materials Reliability Division of the Materials Science and Engineering Laboratory. It summarizes the principal accomplishments in three general research areas: materials performance, properties, and processing. The Fracture Mechanics, Fracture Physics, Nondestructive Evaluation, and Composite Materials Groups work together to detect damage in metals and composite materials and to assess the significance of the damage with respect to service performance. The Cryogenic Materials and Physical Properties Groups investigate the behavior of materials at low temperature and measure and model the physical properties of advanced materials, including composites, ceramics, and the new high-critical-temperature superconductors. The Welding and Thermomechanical Processing Groups investigate the nonequilibrium metallurgical changes that occur during processing and affect the quality, microstructure, properties, and performance of metals.

The report lists the division's professional staff, their research areas, publications, leadership in professional societies, and collaboration in research programs with industries and universities.

12. KEY WORDS (6 TO 12 ENTRIES; ALPHABETICAL ORDER; CAPITALIZE ONLY PROPER NAMES; AND SEPARATE KEY WORDS BY SEMICOLONS)
composites; cryogenic materials; fracture; metallurgy; nondestructive evaluation; physical properties; steels; thermomechanical processing; welding

13. AVAILABILITY

X	UNLIMITED
	FOR OFFICIAL DISTRIBUTION. DO NOT RELEASE TO NATIONAL TECHNICAL INFORMATION SERVICE (NTIS).
	ORDER FROM SUPERINTENDENT OF DOCUMENTS, U.S. GOVERNMENT PRINTING OFFICE, WASHINGTON, DC 20402.
X	ORDER FROM NATIONAL TECHNICAL INFORMATION SERVICE (NTIS), SPRINGFIELD, VA 22161.

14. NUMBER OF PRINTED PAGES
96

15. PRICE
A05

ELECTRONIC FORM